https://doi.org/10.5194/acp-2022-501
Preprint. Discussion started: 29 August 2022

Atmospheric Chemistry and Physics Discussions

An attribution of the low single-scattering albedo of biomass-burning aerosol over the southeast Atlantic

Amie Dobracki[1], Paquita Zuidema[1], Steve Howell[2], Pablo Saide[3], Steffen Freitag[2], Allison C. Aiken[4], Sharon P. Burton[5], Arthur J. Sedlacek III[6], Jens Redemann[7], and Robert Wood[8]

[1]Department of Atmospheric Sciences, Rosenstiel School, University of Miami, Miami, Florida, USA
[2]University of Hawai'i at Mānoa, Honolulu, Hawaii, USA
[3]University of California Los Angeles, Los Angeles, California, USA
[4]Earth and Environmental Sciences Division, Los Alamos National Laboratory, Los Alamos, New Mexico, USA
[5]NASA Langley Research Center, Hampton, VA, USA
[6]Brookhaven National Laboratory, Upton, New York, USA
[7]University of Oklahoma, Norman, Oklahoma, USA
[8]University of Washington, Seattle, WA, USA

Correspondence: Paquita Zuidema (pzuidema@miami.edu) and Amie Dobracki (amie.dobracki@rsmas.miami.edu)

Abstract. Aerosol over the remote southeast Atlantic is some of the most sunlight-absorbing aerosol on the planet: the *in-situ* free-tropospheric single-scattering albedo at the 530 nm wavelength (SSA_{530nm}) ranges from 0.83 to 0.89 within ORACLES (ObseRvations of Aerosols above CLouds and their intEractionS) aircraft flights from late August-September. Here we seek to explain the low SSA. The SSA depends strongly on the black carbon (BC) number fraction, which ranges from 0.15 to 0.4. Organic aerosol (OA) to BC mass ratios of 8-14 and modified combustion efficiency values > 0.975 point indirectly to the dry, flame-efficient combustion of primarily grass fuels, with back trajectories ending in the miombo woodlands of Angola. The youngest aerosol plume, aged 4-5 days since emission and sampled directly west of Angola, broadly consisted of two plumes, with the higher, thicker plume transported more quickly off of the continent by stronger winds. The particle size and fraction of BC-containing particles increased with chemical age, consistent with vapor condensation and coagulation. The particle volume and OA:BC mass ratio reduced simultaneously, attributed primarily to evaporation through photochemistry rather than dilution or thermodynamics. The CLARIFY (CLoud-Aerosol-Radiation Interaction and Forcing: Year-2017) aircraft campaign held near the more remote Ascension Island in August-September 2017 report higher BC number fractions, lower OA:BC mass ratios, lower SSA yet larger mass absorption coefficients compared to this study's. Values from the one analyzed ORACLES-2017 flight, held midway to Ascension Island, are intermediate, confirming the long-range changes. Inorganic ammonium nitrate, thought responsible for the vertical structure in SSA at Ascension Island through thermodynamic gas-particle partitioning, increases from ∼20% of the total nitrate in the ORACLES September flights, to 50% for the August 2017 ORACLES flight midway to Ascension. Overall the data are consistent with continuing oxidation through fragmentation releasing aerosols that subsequently enter the gas phase, reducing the OA mass, rather than evaporation through dilution or thermodynamics. The data support the following best-fit: SSA_{530nm}=0.801+0055*(OA:BC) (r = 0.84). The fires of southern Africa emit approximately one-third of the world's carbon; the emitted aerosols are distinct from other regional BBAs and their aerosol composition also needs to be represented appropriately to realistically depict regional aerosol radiative effects.

https://doi.org/10.5194/acp-2022-501
Preprint. Discussion started: 29 August 2022

Atmospheric Chemistry and Physics Discussions

1 Introduction

Biomass burning, the largest source of carbon to the atmosphere globally, is fundamental to the Earth's global carbon cycle (Bowman et al., 2009; Bond et al., 2013). The emissions include carbon monoxide, carbon dioxide, methane and carbonaceous aerosols, significantly altering the atmospheric composition over large regions of the globe (Andreae, 2019). This in turn influences all of the gaseous, aerosol and aerosol-cloud interaction radiative forcing terms considered within the IPCC Assessments. Despite the importance of biomass burning events on climate, smoke properties after long-range transport are still poorly characterized. These include the effluents from northern European and Russian forest fires reaching the Arctic basin (Cubison et al., 2011), wildfire smoke from western continental north America observed over Europe (Zheng et al., 2020; Baars et al., 2021), and aerosols from fires in southern Africa reaching south America (Holanda et al., 2020). Without wet or dry scavenging, the aerosol's areal coverage is increased through transport, increasing the aerosol's radiative impact.

Southern Africa region produces approximately one-third of the world's fire-emitted carbon (van der Werf et al., 2010). The global maximum of absorbing aerosol above cloud occurs above the southeast Atlantic (Waquet et al., 2013), a combination that produces a direct radiative warming of the regional climate (Keil and Haywood, 2003; Graaf et al., 2014; Zuidema et al., 2016; Mallet et al., 2021; Doherty et al., 2022). Biomass-burning aerosol (BBA) from this region is unusual for being highly absorbing of sunlight, with SSA values of 0.85 or less at the green wavelength (Zuidema et al., 2018; Chylek et al., 2019; Pistone et al., 2019; Holanda et al., 2020; Taylor et al., 2020; Denjean et al., 2020b; Mallet et al., 2020; Shinozuka et al., 2020; Carter et al., 2021; Brown et al., 2021). More absorbing aerosol will reduce the need for latent heat release within the world's energy balance (Pendergrass and Hartmann, 2012) and alters regional circulation and precipitation patterns (Mallet et al., 2020; Solmon et al., 2021; Chaboureau et al., 2022). While climate models discern an ensemble-mean direct radiative warming, individual models disagree strongly on magnitude and even sign (Myhre et al., 2013; Zuidema et al., 2016; Haywood et al., 2021; Mallet et al., 2021). In addition, the direct aerosol radiative effect estimated from satellites typically exceeds model estimates (de Graaf et al., 2020). That the measured SSAs are lower than what is currently implemented in many models (Shinozuka et al., 2020; Mallet et al., 2021; Doherty et al., 2022), suggests one cause for an underestimated modeled direct radiative warming is a model SSA that is too high.

This study's goal is to examine the optical properties and composition of *in-situ* smoke sampled during six flights of the NASA Earth Venture Suborbital-2 ORACLES (ObseRvations of Aerosols above CLouds and their intEractionS; Redemann et al., 2021) deployment, primarily from September, 2016 (Fig. 1). The flights occur within 30 days of each other in the seasonal cycle, to select for similar composition of the fire source emissions. One flight, on 9/24/2016, expressly sampled a thick, younger aerosol plume closer to the African continent (Fig. 2). Another flight, on 8/31/2017, occurred midway to Ascension Island and overlapped with the UK CLARIFY (CLoud-Aerosol-Radiation Interaction and Forcing: Year-2017) aircraft campaign (Haywood et al., 2021) on Ascension Island (8°S, 14.5°W), held from August 17 - September 7, 2017. The 8/31/2017 flight data provide an opportunity to indirectly assess how smoke may evolve as it advects further westward.

This study's primary explanation for why biomass-burning aerosol (BBA) is so highly absorbing of sunlight is a high black carbon content in both the number and mass of total particles, as already shown in Taylor et al. (2020) and Denjean et al.

https://doi.org/10.5194/acp-2022-501
Preprint. Discussion started: 29 August 2022


Atmospheric Chemistry and Physics Discussions

(2020b). We further strengthen the attribution to aerosol composition, fire source characteristics and indicators of chemical aging. Data from the 9/24/2016 flight, the one flight with consistent BC:CO ratios as a function of a chemical aging marker, 4-5 days after emission, further connects changes in aerosol composition to coagulation and condensation processes, in addition to documenting genuine mass loss, extending an earlier analysis of the same flight presented within Dobracki et al. (2022). Level-leg measurements, with their lower uncertainties, demonstrate how optical properties relate to chemical and physical composition, and can be compared to published values from Wu et al. (2020) and Taylor et al. (2020) made at Ascension Island, to examine potential aging impacts. A caveat remains the limitation that measurements are made in different locations at non-Lagrangian times. We seek to mitigate this through also examining the influences that can be indirectly attributed to the fire sources. This study complements that of Wu et al. (2020), who examined more fully aged aerosol at Ascension Island and concluded that the single-scattering albedo vertical structure is primarily explained by a thermodynamical repartioning of inorganic nitrate to the particle phase at cooler and moister altitudes aloft. We therefore examine inorganic nitrate fractions as well. Further focus on data from the 8/31/2017 flight, added since Dobracki et al. (2022), helps connect interpretations of ORACLES versus CLARIFY aerosol characteristics.

2 Datasets

The more technical details of the datasets and sampling layout are provided in the Supplement, with the information that is more central to the conclusions of this study provided here. This also includes references to results from the ORACLES-CLARIFY intercomparison flight held on 18 August, 2017 (Barrett et al., 2022), within a smoky boundary layer and clean free troposphere, where relevant.

2.1 Determination of physical aerosol age

All of the flights occurred over the ocean far from the fire sources. One approach for estimating the physical age relies on model-released tracers tagged to carbon monoxide (CO) at the fire source for each day of the campaign's operational two-week aerosol forecast, made using the Weather Research and Aerosol Aware Microphysics (WRF-AAM) Model (Thompson and Eidhammer, 2014). The current analysis takes advantage of the model's prior use seeking out smoke layers to sample during the aircraft campaign. The model fire source is a burned area product of 500 m spatial resolution from the Moderate Resolution Imaging Spectrometer (Giglio et al., 2006) and may miss up to $\sim$ 40% of the total burned area (Ramo et al., 2021). Other work suggests that larger fires contribute more to the emissions reaching higher altitudes for the boreal northern hemisphere (Martin et al., 2010), where the aerosols are more readily transported offshore. We are unsure how well this same vertical redistribution applies for the smaller agricultural fires of southern Africa. The regional model has a12-km spatial resolution and encompasses a domain (41°S-14°N, 34°W-51°E) sufficiently large to capture almost all contributing fires (Saide et al., 2016). The model is driven by the National Center for Environmental Prediction Global Forecasting System (NCEP GFS) meteorology, using daily smoke emissions from the Quick Fire Emissions Dataset (Darmenov and da Silva, 2013) released into the model surface layer. These are advected thereafter according to the model physics, with their spatial distribution constrained near real-time with

https://doi.org/10.5194/acp-2022-501
Preprint. Discussion started: 29 August 2022


Atmospheric Chemistry and Physics Discussions

satellite-derived optical depths. This allows a diurnal cycle representation of the daytime burning. The tracer-derived estimates include a tendency for the smoke emissions to initially remain near the surface until carried aloft up to 4-5 km, shown for 24 September 2016 in Fig. S4. This process will mix the emissions from nearby fire sources, homogenizing local differences in, e.g., grass versus leaf-litter contributions, moisture content, and surface burn history. Conditions can nevertheless still change from day to day. Backtrajectories based on the HYSPLIT model (Stein et al., 2015), driven by the same NCEP GFS meteorology, further illuminate the pathway taken by the BBA. The backtrajectories typically generate younger aerosol age estimates, because the time needed for the vertical transport is unaccounted for.

2.2 Modified combustion efficiency

CO and CO_2 are used to infer fire emission conditions through the modified combustion efficiency (MCE) metric (Collier et al., 2016; Yokelson et al., 1997):

$$MCE = \frac{\Delta CO_2}{\Delta CO + \Delta CO_2} = \frac{1}{1 + \Delta CO/\Delta CO_2} \quad (1)$$

Higher values of MCE (>0.9) are associated with flaming combustion, which preferentially produce more BC, whereas values less than 0.9 are more typical of smoldering combustion, which can emit more organic aerosol for the same amount of fuel (Yokelson et al., 2009; Vakkari et al., 2018). A regression is used to estimate the $\Delta CO/\Delta CO_2$ with ΔCO and ΔCO_2 calculated from the measured CO and CO_2 amounts, in moles, relative to background values. Adopted background values were 65 (77) ppbv for CO, and 397 (404) ppmv for CO_2, in September 2016 (August 2017), based on measurements in the free troposphere taken above the smoke plumes (∼7000 m).

2.3 Aerosol Composition

Black carbon mass and number concentrations are derived from a 4-channel single particle soot photometer (SP2, Droplet Measurement Technology) deployed by the Hawaii Group for Environmental Aerosol Research HiGEAR in 2016, and an 8-channel SP2, of which only the incandescent channels were functional for the August 31, 2017 flight, deployed by Art Sedlacek of Brookhaven National Laboratory. The intensity of laser-induced incandescent emission at 1064 nm can be quantitatively related to the mass of the refractory black carbon particles, for mass-equivalent diameters between approximately 80-500 nm. The SP2 was calibrated using fullerene soot, using effective density estimates from Gysel et al. (2011). A nominal mass uncertainty of ± 17% is applied following Laborde et al. (2012), primarily driven by calibration uncertainty. No scattering data are available, precluding information on coating thicknesses. Ratios of $\frac{\Delta BC}{\Delta CO}$ serve to assess homogeneity of the aerosol composition at the source emission. Because the background BC is zero in clean conditions, the ratio reduces to $\frac{BC}{\Delta CO}$. The ratios are non-dimensionalized by using the ideal gas law at standard temperature (273K) and pressure (1000 hPa) to convert the CO concentrations from ppb to ng m^{-3}.

HiGEAR operated an Aerodyne High-Resolution Time-of-Flight Aerosol Mass Spectrometer (HR-ToF-AMS, referred to as AMS), building on previous experience in the southeast Pacific (Yang et al., 2011; Shank et al., 2012) and the Arctic (Howell et al., 2014). The native time resolution is approximately five seconds, sampling two seconds at a time, with the data

https://doi.org/10.5194/acp-2022-501
Preprint. Discussion started: 29 August 2022


Atmospheric Chemistry and Physics Discussions

interpolated onto a one-second temporal grid to facilitate integration with other datasets. The overall uncertainty in the reported aerosol mass concentrations is estimated at 33% to 37%, at a one-minute time resolution, based on Bahreini et al. (2009). Some analyses were restricted to level legs ranging from 4 to 10 minutes, inidividually listed in Table S2. This further reduces the uncertainty about the mean to 19%-10 %. The combined uncertainty in the organic aerosol (OA) to BC mass ratios is then close to 40%, reducing to 25%-19% for the level legs. Since the background OA in clean conditions is also zero, $\frac{\Delta OA}{\Delta BC}$ reduces to OA:BC. The instrument inter-comparison flight with CLARIFY sampled a clean troposphere but a polluted boundary layer (BC of $\sim$ 300 ng m^{-3}), during which the ORACLES OA and nitrate mass concentrations were 80% of those measured by the UK plane, but within each other's standard deviations (Barrett et al., 2022).

The uncertainty in OA is expected to be smaller when aerosol concentrations are larger, in part because of improved signal-to-noise. Larger aerosol concentrations, sampled from within the heart of the smoke plumes, are also less subject to dilution effects, by which OA evaporates through mixing with cleaner environmental air (e.g., Hodshire et al., 2021), and from model-observational disparities in the smoke plume locations, which are likely to be larger at the smoke plume edges. The OA:BC mass ratio is significantly less for air with OA>3 μg m^{-3} than for air with OA>20 μg m^{-3}, particularly for younger aerosol (Fig. S5a). Although evaporation of OA through dilution at lower OA masses could explain this, the OA is not volatile, as shown later, so that this relationship requires a different explanation. The OA:BC mass ratio stabilizes at OA mass concentrations $\geq$ 20 μg m^{-3} (Fig. S5b), establishing the threshold we apply throughout this study. Fig. S5a also indicates OA:BC mass ratios can increase again 10 days after emission, but we exclude such old aerosol as the model skill in the smoke age is likely to become less over time. The choice of threshold is inherently arbitrary, and some analysis is repeated using an OA>10 μg m^{-3} threshold to make sure our findings are not sensitive to the choice of OA mass threshold. An additionally-applied approach to removing dilution effects is to normalize with respect to BC or ΔCO. We stress, however, that the aerosol plumes are typically much larger and homogeneous than those sampled from fires in the western northern hemisphere, which are often named, individual fires sampled close to the source. Dilution of the aerosol plume is much less of a concern during smoke-filled conditions over the southeast Atlantic. The OA mass concentrations are often highly stable during the individual level legs (Table S2), with 20 minutes of data reducing the absolute (relative) uncertainty in the OA mass concentration to at most 1.6 μg m^{-3} (8%).

Measurements of *f44*, the fraction of the OA mass spectrum signal at *m/z 44* relative to the total OA mass concentration, indicates the presence of the CO_2^+ ion, a form of oxidation resulting from chemical aging (Canagaratna et al., 2015). *f43* is the fraction of the OA mass spectrum signal at *m/z 43* (C_2H_3O+ and $C_3H_7^+$) and is also representative of oxygenated OA. *f60*, the fraction of the OA mass spectrum signal at *m/z 60* ($C_2H_4O_2$), is a fragment of levoglucosan, a known tracer for biomass burning aerosol (Cubison et al., 2011). Elemental analysis, yielding hydrogen (H), oxygen (O) and organic carbon (OC) rely on algorithms within Aiken et al. (2007). The calibration constants differ between the two years but this change does not quantitatively impact any differences shown here.

2.4 Determination of organic/inorganic nitrate contribution

Farmer et al. (2011) provide an approach for estimating the contribution to the total nitrate signal from organic nitrate (ON) using the $NO^+ : NO_2^+$ ratio, building on the observation that organic nitrates typically fragment into larger proportions of

https://doi.org/10.5194/acp-2022-501
Preprint. Discussion started: 29 August 2022


Atmospheric Chemistry and Physics Discussions

NO^+ than do inorganic nitrates (INs; in their study, organic NO^+ ratios vary between 1.8 to 4.6 for different organonitrates, compared to 1.5 for NH_4NO_3). Their Equation 1, reproduced below, provides an estimate of the ON fraction that can be readily applied to the ORACLES AMS data, assuming enough ON is present that it can be resolved. The success of this approach also assumes that the inorganic nitrates capable of providing a large NO^+ ratio, such as mineral nitrates, are not present. Both assumptions are justified for the SEA free troposphere.

$$X(ON\%) = \frac{(R_{obs} - R_{NH_4NO_3})(1 + R_{ON})}{(R_{ON} - R_{NH_4NO_3})(1 + R_{obs})} \quad (2)$$

R_{obs} is the ORACLES *m/z* ratio of ion fragments 30 to 46, $R_{NH_4NO_3}$ is the ionization efficiency (IE) calibration-derived ratio (1.26 for 2016 and 1.545 for 2017) and an R_{ON} value of 3.41 is a reference ratio based on the average fragmentation pattern into the $NO^+ : NO_2^+$ ratios for the OIA-HN, OIA-CN and OIA-olig standards evaluated within Table S1 of Farmer et al. (2011). The inorganic nitrate (IN) fraction is 1-ON. We use this approach to estimate the IN (primarily NH_4NO_3) fraction, keeping in mind that it is an indirect inference. The CLARIFY campaign relied on assessing *m/z* 30 (NO^+) and *m/z* 46 (NO_2^+) to assess the organic to inorganic nitrate contribution.

2.5 Aerosol sizing

We rely on aerosol particle size estimates from the long differential mobility analyzer (LDMA; TSI 3071A), the thermal DMA (TDMA), the Ultra-High Sensitivity Aerosol Spectrometer (UHSAS; DMT), two condensation counters (CNs) and the SP2. The LDMA measures mostly singly-charged particles between 10-550 nm. The HiGEAR LDMA operated in a scanning mode at ambient temperature and pressure, drawing in desiccated air (RH<30%) from an aluminum lagged-aerosol grab chamber for 60 seconds. The total uncertainty is estimated to be ± 30 % due to errors in sizing of non-spherical particles along with uncertainties of flow rate.

The UHSAS optical spectrometer measures particles between 60-1000 nm at a higher one-second time resolution. An infrared laser illuminates particles, with the scattered light collected on two pairs of optical detectors. The particle sizes are then divided into 100 user-specific size bins. The UHSAS undersizes almost 30% of black carbon containing particles during ORACLES (Howell et al., 2021), because of refractive indices assumptions. A correction for the undersizing is evaluated in Fig. S6 against the LDMA median diameters within smoke plumes with OA>20 μg m^{-3}. For the larger particles containing BC, the UHSAS correction reduces the undersizing bias to 15% for LDMA median diameters $>$ 150 nm, but for the smaller particles that are less likely to contain BC, the UHSAS particle sizes are now overcorrected. For this reason we only show results for the LDMA data; UHSAS data do not contradict our findings. All size distributions and concentrations are corrected to STP (T=25˚C, 1013mb).

The number of BC-containing particles is provided relative to particle cavity aerosol spectrometer probe (PCASP; 100-3000nm) number concentrations in Wu et al. (2020), and the ORACLES and CLARIFY PCASP number concentrations agreed to within 10% during the intercomparison flight (Barrett et al., 2022). Nevertheless, the ORACLES PCASP performance was variable throughout the three-year campaign, and did not compare as anticipated to the CN and LDMA number concentrations during ORACLES-2016. For this reason, we report the number of BC-containing particles relative to the LDMA number con-

https://doi.org/10.5194/acp-2022-501
Preprint. Discussion started: 29 August 2022


Atmospheric Chemistry and Physics Discussions

centrations throughout. The CN (TSI 3010) counter apply a lower size threshold of 10 nm, with no upper bound, and provides the most complete aerosol number concentrations. An independent measure of aerosol volatility is assessed by comparing the size distributions heated to 150° within the TDMA to the unheated size distribution. The TDMA has an upper size-cutoff of 0.18-0.2 μm and will not see the larger BC particles. An estimate of the black carbon core mass-median diameter is also calculated from the SP2-provided mass and number concentrations, assuming a BC density of 1.8 g cm^{-3} (Bond and Bergstrom, 2006). This inversion is specific to the range of BC sizes that the SP2 is sensitive to, but comparisons of this metric across flights helps support an attribution to the fire source, as larger BC sizes are found to correspond to more woody fuels than grasses (Holder et al., 2016).

2.6 Optical Measurements

Scattering from all particles is measured continuously by a TSI nephelometer (model 3563) at the (450, 550, 700) nm wavelengths (λ), with a linear regression in log-log space used to estimate the scattering at λs of 470, 530 and 660 nm. The spectral light absorption coefficients (σ_a) of the total aerosol are measured by a Particle Soot Absorption Photometer (PSAP; Radiance Research) at the (470, 530, and 660) nm wavelengths. The algorithmic treatment of these filter-based measurements is provided in the Supplement. The extinction and absorption measurements compare well at the blue and green wavelengths to the more sophisticated measurements made by the CLARIFY EXtinction SCattering and Absorption of Light for AirBorne Aerosol Research (EXSCALABAR) instrument (Davies et al., 2019; Barrett et al., 2022).

The absorption Angstrom exponent (AAE) values are calculated from the linear fit of $\log(\sigma_a)$ to $\log(\lambda)$. The mass absorption cross-section (MAC) measurements are based on the absorption coefficient divided by the BC mass concentration. Following Carter et al. (2021), we also evaluate the MAC relative to the BC+OA mass concentration at a λ of 470 nm. At λ=660 nm, the solar absorption will be dominated by the black carbon, whereas at λ=470 nm the MAC_{BC+OA} will contain contributions from both OA-induced brown carbon as well as other wavelength-dependent absorbers (Zhang et al., 2022).

3 Data Selection

Data selection is based on the availability of at least 20 minutes of OA data exceeding $>$20 μg m^{-3} at altitudes above 1.5 km and relative humidities (RH) $<$ 80%, for which model-derived ages span up to 10 days. Towards improving the likelihood of sampling from similar aerosol source regions, only flights spanning August 31 through all of September for 2016 (5 flights) and 2017 (one flight) are considered, shown relative to the satellite-derived above-cloud aerosol optical depths for September 2016 in Fig. 1. Aerosol forecast maps indicate the spatial sampling of the aerosol plumes for each flight, with the OA data and model-estimated age displayed on individual altitude-latitude flight track projections (Figs. S7-S8).

The aircraft either flew along a routine southeast to northwest track (31 August, 4 and 25 September of 2016), or, performed target-of-opportunity flights sampling more aerosol-rich locations (6 and 24 September of 2016, 31 August 2017). The flight tracks make clear that the aircraft sampled widely, but never near the fire emission sources, with the 9/24/2016 flight coming closest (Fig. 2). The aerosol spatial distribution is strongly influenced by the strength of the free-tropospheric easterly winds,

https://doi.org/10.5194/acp-2022-501
Preprint. Discussion started: 29 August 2022


Atmospheric Chemistry and Physics Discussions

and is either constrained to near the coast, or elongated zonally along 10°S (Figs. S7-S8). On the 24-25 September 2016 and 31 August 2017 flights, the zonal easterly winds exceeded 6 m s^{-1} along $\sim$ 10°S at altitudes between 3-5 km, forming a wind isotach known as the African Easterly Jet-South (Nicholson and Grist, 2003; Adebiyi and Zuidema, 2016). Overall, September 2016 was climatologically representative (Ryoo et al., 2021), with more synoptic detail available in Ryoo et al. (2022).

The different flights intersect air of different ages, but all model-estimated ages exceed 4 days. The aerosol sampled during the Southern African Regional Science Initiative (SAFARI) campaign (Haywood et al., 2003) held in 2002 near Namibia was less than 2-3 days of age, while the CLARIFY-2017 campaign over Ascension sampled aerosol approximately a week old (Wu et al., 2020; Taylor et al., 2020). The ORACLES-2016 model-derived age estimates place the flights uniquely within the time record available on chemical aging over the southeast Atlantic (with the caveat that the age-determination protocol may vary between campaigns). The two flights we highlight further are from 9/24/2016, because of its objective to sample within a thick smoke plume as close as possible to a fire emission source, and the 9/31/2017 flight, which sampled an aerosol layer of significant mass and extremely stable OA:BC, and occurred halfway to Ascension during the CLARIFY time period.

Table S1 lists all of the ORACLES-2016 flights and includes comments on their flight pattern, the number of seconds with OA>20 g m^{-3}, and other selection considerations. Table S2 provides flight dates, location, time span and altitude of the level legs.

4 Chemical composition and age distribution within the six flights

The mean submicron mass fractions of the six flights combined are 66% OA, 10% nitrate (NO_3), 11% sulfate (SO_4), 5% ammonium (NH_4), and 8% BC, with the masses for each species and flight in Fig. 3, thresholded for OA $>$ 20 g m^{-3}. Flight-mean submicron mass totals typically exceed 35 μg m^{-3}, much more than measured during CLARIFY (Wu et al., 2020), and are dominated by OA.

Fig. 4 provides an overview of the *f44*, OA to BC mass ratio, model-derived time since emission (age), modified combustion efficiency (MCE), non-dimensionalized $\frac{BC}{\Delta CO}$ ratios and ozone values for each flight. *f44* flight-mean values range from 0.18 to 0.22, with the youngest aerosol from the 9/24/2016 flight also possessing the lowest flight-mean *f44* value. The values are on par with *f44* values from Asian/Siberian smoke transported to Alaska during two weeks (Cubison et al., 2011), indicating highly-oxidized aerosol. They are also similar to CLARIFY values (Wu et al., 2020), suggesting a maximum *f44* value of $\sim$ 0.22 for this aerosol regime. Flight-mean OA:BC mass ratios range from 7 to 13, possibly increasing throughout the month. Modified combustion efficiency values are above 0.97 for each flight, clearly indicating flame-efficient fires (Collier et al., 2016; Zhou et al., 2017) and exceeding the September-mean estimate of $\sim$ 0.89 in Zheng et al. (2018) using a model based on source emissions. The high MCE values could reflect a sampling bias favoring sampling the most intensive plumes, or, that the smoke from the most intense fires is more easily dispersed. Mean non-dimensionalized $\frac{BC}{\Delta CO}$ ratios vary between 0.007 to 0.011, with a minimum on 24 September. These ratios are among the highest surveyed in the literature (Table 1). Overall, $\frac{BC}{\Delta CO}$ ratios do not increase with increasing MCE as expected based on Kondo et al. (2011), but this likely reflects this study's small range of MCE values, for which Vakkari et al. (2018) also do not find a correlation. The mean $\frac{BC}{\Delta CO}$ values hint at a decrease

https://doi.org/10.5194/acp-2022-501
Preprint. Discussion started: 29 August 2022


Atmospheric Chemistry and Physics Discussions

throughout September, consistent with the speculation that the more combustible fuel is ignited earlier (Eck et al., 2013), but the trend is statistically-insignificant. The flight-mean OA:BC mass ratios also increase from $\sim$ 10 to 13 later in September. The flight-mean ozone levels range from 80-105 ppbv, possibly decreasing as September progresses. Flights with more ozone correspond to flights with lower MCEs. This is expected as slightly less flaming fires will also emit more ozone along with more OA. Flight-mean aerosol ages of 4 to 10 days since emission (Fig. 4c) do not clearly correlate to the other metrics.

We interpret the high MCE values to reflect a large contribution from dry and dead grasses, rather than green grass or more woody materials, for the following reasons. MCE varies inversely with the moisture content for grasses (Korontzi et al., 2003), with leaf litter and woody fuels tending to dry more slowly than do grasses. For this reason woody fuels are more prone to smoldering than flaming combustion. The burning of dry grass produces relatively low emissions of carbon monoxide (Scholes et al., 1996) and higher emissions of black carbon than agricultural or woodland fires (Andreae, 2019), elevating the $\frac{BC}{\Delta CO}$ ratios, as seen here (Table 2). That the $\frac{BC}{\Delta CO}$ values measured at offshore locations exceeds those measured previously over land (Table 2) could be because emissions from more intense, larger, flaming fires can more easily reach higher altitudes (Martin et al., 2010; Holder et al., 2016), where they can be dispersed further afield through the stronger winds aloft.

Daily maps of fire locations for the flight days (not shown, see Redemann et al. (2021) for the monthly-mean distributions) indicate the BBA sources are primarily fire emissions from miombo woodlands, which contain a significant fraction of savanna grasses and some agricultural fields (Shea et al., 1996; Christian et al., 2003; Korontzi et al., 2003; Vakkari et al., 2018; Huntley, 2019), distributed over a broad geographic region encompassing Angola, Zambia and the Congo. The miombo shrubbery is fire-adapted and less likely to burn than grass. A survey of the published emission factors for the vegetation types typical of southern Africa - savannahs, grasslands, agricultural fields, and at times tropical forest (Table 1) indicates that the high $\frac{BC}{\Delta CO}$ ratios reported in Table 2 and Fig. 4 are primarily representative of grass fires. Overall, these metrics indicate aged, oxidized aerosol emanating from flame-efficient fires, without any strong outliers amongst the flights (flight-mean $\frac{BC}{\Delta CO}$ ratios vary from 7-11*10^{-3}), typical values for grasslands and savannahs (Janhäll et al., 2010; Vakkari et al., 2018).

Southern African fires can still produce significant near-source secondary organic aerosol (SOA), depending on the burning conditions (Vakkari et al., 2018; Pokhrel et al., 2021). The comparison of *f44* to *f43* for all the flights (Fig. 5a) indicates a mixture of semi-volatile and low-volatile oxygenated organic aerosol (Ng et al., 2011). A PIKA analysis reveals the dominant peak at *f43* is from $C_2H_3O^+$, representative of oxygenated organic aerosol (Ng et al., 2011). *f60* values are relatively constant and below 0.005 (Fig. 5b), and *f44* values lie between 0.2 and 0.22. Chamber studies report lifetimes for *f44* and *f60* of approximately 20 days and 10 hours, respectively (George and Abbatt, 2010; Hodshire et al., 2019), but little change is evident in *f44* after 6 days since emission (Fig. 5c, with *f44* values of 0.2-0.22 also reported at Ascension (Wu et al., 2020), suggesting a steady state has been reached.

Flight-mean O:C mass ratios range between 0.61 to 0.69 for the 2016 flights, with small within-flight standard deviations (0.03-0.06, not shown). Overall, the average ($\pm$ standard deviation) plume values of H:C, O:C, and the organic-aerosol-to-organic-carbon mass ratio (OA:OC) are 1.2 $\pm$0.1, 0.7 $\pm$0.1, and 2.2$\pm$0.1, respectively, over all six flights. The H:C and O:C values align well with airborne oxidized OA values measured around Mexico City during the Megacity Initiative: Local and Global Research Observations (MILAGRO) campaign (Heald et al., 2010). The OA:OC mass ratio, a measure of the oxygen

https://doi.org/10.5194/acp-2022-501
Preprint. Discussion started: 29 August 2022


Atmospheric Chemistry and Physics Discussions

content that is useful for model evaluation (Hodzic et al., 2020; Lou et al., 2020), are on par with measurements from the Atmospheric Tomography (ATom) campaign made in the same region (Hodzic et al., 2020) and at Ascension Island during the CLARIFY campaign (Wu et al., 2020), and higher than common model-applied values of 1.4-1.8 (Aiken et al., 2008; Tsigaridis et al., 2014; Hodzic et al., 2020) and of primary near-source OA:OC ratios of 1.6 (Andreae, 2019).

The H:C versus O:C mass ratios occur close to the -1 slope line (Fig. 6; based on vanKrevelen (1950)), also inferred at Ascension (Wu et al., 2020). This slope relationship is common to many laboratory and field studies (Heald et al., 2010), with the narrow distribution, particularly within individual flights, suggesting either a limit to the number of oxidation pathways and molecular structures, or, a dominant few. Most of the oxidation states (OS), defined as 2*O:C-H:C (Kroll et al., 2011), lie between -0.2 and 0.5, which Kroll et al. (2011) categorize as "aged" (OS between 0 and 0.5) and semi-volatile oxygenated OA (OS between -0.5 to 0). Only the 31 August, 2017 flight has some aerosol that is oxidized enough to be considered low-volatile (OS $>$ 0.5), even more than aerosol from MILAGRO (Heald et al., 2010). We are only able to report the end product of the aerosol chemical properties, and different SOA precursors may also contribute to the range of the observed H:C and O:C ratios (Jimenez et al., 2009; Ng et al., 2011). Nevertheless, Kroll et al. (2009) show aerosol with O:C $>$ 0.4 are dominated by fragmentation pathways, in which further oxidation occurs through the loss of a carbon atom (as opposed to functionalization, which adds an oxygen atom). Fragmentation generates relatively small changes in H:C, which could explain the small increase in scatter evident for the lowest-volatile aerosol. The fragmentation process releases small amounts of volatile aerosol and we speculate this pathway is suggested by Fig. 6 for the continuing oxidation of ORACLES-2016 BBA.

5 Optical and Physical Properties

Here we discuss relationships between the aerosol optical properties to their chemical and physical composition, and examine their spatial distribution, using the more statistically-robust level-leg mean ($\pm$ standard deviations) values (Figs. 7-9).

5.1 Mean Relationships

Absorption of sunlight primarily depends on BC, and as expected, the bulk mass absorption coefficients (MAC_{660nm}) and SSA values depend to first-order on an estimate of the fraction of particles containing black carbon, defined as the number of SP2-derived BC particles divided by the LDMA total particles (FrBC; Fig. 7a and b). The BC-containing particle fraction varies from 0.2 to 0.4, more than the 0.1-0.2 range shown for July (Denjean et al., 2020b), and less than at Ascension (Taylor et al., 2020). The total particle number was drawn from the full aerosol size distribution within Denjean et al. (2020b), and by a PCASP (0.1 μm-3μm) at Ascension, but as shown later few aerosol particles exceed the 550 nm upper size limit of the LDMA.

Electron microscopy shows almost all BC is at least partially coated, meaning the BC is internally mixed (Dang et al., 2022). Nevertheless, the majority of particles do not include BC. As the fraction of BC-containing particles increase, the bulk OA:BC mass ratio tends to decrease. MAC_{600} ranges from 9-12 m^2 g^{-1}, and MAC_{470} from 13-18 m^2 g^{-1}, corresponding to absorption enhancement factors of 1.2-1.6 (1.7-2.4) at the 660 nm (470 nm) wavelengths, assuming an MAC of 7.5 m^2 g^{-1} for uncoated black carbon (Bond and Bergstrom, 2006) (and greatly exceeding the MAC value of 6.25 m^2 g^{-1} for strongly light-absorbing

https://doi.org/10.5194/acp-2022-501
Preprint. Discussion started: 29 August 2022


Atmospheric Chemistry and Physics Discussions

carbon (Bond and Bergstrom, 2006)). The mean MAC_{660} of 10.8 m^2 g^{-1} is slightly higher than the median value of 9.3 m^2 g^{-1} reported in Carter et al. (2021), likely because the BC-enriched 31 August 2017 flight contributes strongly to the mean value reported here. Median LDMA-inferred particle diameters range from 120-210 nm, with no clear relationship to MAC_{470}. This indicates the absorption enhancements are governed more by composition than particle size, also concluded by Denjean et al. (2020a) for June-July BBA close to the near-equatorial African coast. The 8/31/2017 flight, for an FrBC of 0.3, has a higher MAC_{660nm} (by $\sim$ 2 m^2 g^{-1}), lower OA:BC mass ratio, larger particle/BC core sizes, and more coating (crudely estimated as the LDMA-BC core diameter difference divided by two, primarily intended as a relative measure), compared to values from the 9/6/2016 flight of comparable FrBC. The larger BC core size for 8/31/2017 may come from a woodier fuel, supported by backtrajectories emanating from further north (not shown). Woodier material can generate larger BC sizes irrespective of MCE (Holder et al., 2016). We do not know how to reconcile a lower OA:BC mass ratio with a thicker coating, however.

The single scattering albedo (SSA) values at λ=530 nm range from 0.83 to 0.89, consistent with the ORACLES-2016 mean SSA of 0.86 (inter-quartile range of $\sim$ 0.028) based on all the flight data (Pistone et al., 2019). These SSA values are lower than previously documented *in situ* values over land or coastal (Haywood et al., 2003; Formenti et al., 2003; Dubovik et al., 2002), on par with AERONET September-mean values at Mognu (Eck et al., 2013),and higher than those reported at Ascension Island (Zuidema et al., 2018; Wu et al., 2020). An SSA best-fit regression on OA:BC provides a straightforward connection between the BBA chemical and optical properties: SSA_{530nm}=0.801+0.0055*(OA:BC) (Fig. 8, correlation coefficient r of 0.84. The dependence on BC:TC following Brown et al. (2021) is: SSA_{530nm}=0.929-0.389*(BC:TC) (Fig. 8b; r=-0.79) using the same calculation for OC (Aiken et al., 2007). The dependence on BC:TC is not as pronounced as in Brown et al. (2021) primarily because our data lack highly-scattering aerosol. The variance in SSA is explained slightly better by OA:BC than BC:TC. The remaining ORACLES-2017 data will support further investigation of these relationships in a follow-up study.

5.2 Is there evidence of brown carbon?

Taylor et al. (2020) place an upper estimate of 11% on shortwave absorption by brown carbon (BrC) at 405 nm wavelength by the time the BBA plume reaches Ascension Island, with . Zhang et al. (2022) indicate that other non-BrC materials absorb sunlight over the southeast Atlantic as a function of wavelength, so that BrC may contribute even less than $<$ 10% of the total. Brown carbon is mostly associated with primary organic aerosol. By four days since emission, the primary organic aerosol that may contribute to wavelength-dependent solar absorption is expected to be gone, with SOA mostly scattering light (Bond and Bergstrom, 2006; Laskin et al., 2015). Ozone Monitoring Instrument UltraViolet Aerosol Index values do suggest OA-produced brown carbon should be present east of the prime meridian (Carter et al., 2021), however. Laboratory studies find more BrC absorption for lower OA:BC mass ratios (Saleh et al., 2014; Holder et al., 2016; McClure et al., 2020), because more intense fires also produce more primary OA/BrC. One important difference is the primary OA fraction and AAEs are high within, e.g., Saleh et al. (2014). Nevertheless, if oxidation can continue to produce new chromophrores (O'Brien and Kroll, 2019) that absorb differently based on wavelength, that could be interpreted as a form of SOA-induced BrC.

Motivated by Carter et al. (2021) we examine if distance from the continent has a detectable influence on the absorption Angstrom exponents (AAE) calculated over the 470-660 nm wavelength range for the same level legs (Fig. 9a). The values

https://doi.org/10.5194/acp-2022-501
Preprint. Discussion started: 29 August 2022


Atmospheric Chemistry and Physics Discussions

span 1.1-1.3 south of 8°S irrespective of distance from the coast, and are close to one further north for the more remote 8/31/2017 flight (Fig. 9a). AAE is weakly but positively correlated with OA:BC (r = 0.27). This is counter to expectations based on Saleh et al. (2014) and McClure et al. (2020), but does suggest that perhaps some of the secondary OA is absorbing of sunlight. An important caveat remains that the 470 nm wavelength may already be too long to be responsive to additional absorption by OA-produced BrC (Zhang et al., 2022). Another assessment of brown carbon absorption can be done using the mass absorption coefficients at 470 nm relative to the sum of the BC and OA mass concentration ($MAC_{470,BC+OA}$; following Carter et al., 2021) (Fig. 9b). These range from 0.94-1.2 m^2 g^{-1} south of 8°S (with one exception) to 1.4-1.7 m^2 g^{-1} further north. $MAC_{470,BC+OA}$ is anticorrelated with OA:BC (r= -0.86). Although consistent with (Saleh et al., 2014), the small sample size, dominated by one flight north of 8°S with less OA:BC, precludes much interpretation (see, e.g., Fig. 7 instead) and we primarily conclude a lack of a longitudinal dependence, but the sample size is too small to say this with confidence. There is some indication that the co-emitted sulfate can contribute to increasing overall absorption (Christian et al., 2003), as can the enhanced humidity present within the aerosol layers (Redemann et al., 2001), but we do not find a correlation between MAC and sulfate fraction.

6 Is there evidence for ongoing loss of organic aerosol? 24 September 2016 case study

The measurements of *f44* only correlate with the model-derived age estimates for 4-6 days (Fig. 4c). The data for the 4-5 days-old aerosol stems from the 9/24/2016 flight (Fig. 2) and we examine that flight's data more closely. Backtrajectories from the profile at 12.3°S, 11°E show the aerosols are coming from similar source regions (Fig. 10d), and become distributed vertically primarily by variations in the advection speed. One main aerosol layer is centered on 5 km, aged ∼4 days since emission, and a slightly older smoke layer of ∼5 days in age is centered on 3 km (Fig. 10b,c). The younger aerosol aloft is connected to stronger upper-altitude winds also transporting moisture, consistent with climatological expectations (Adebiyi et al., 2015; Adebiyi and Zuidema, 2016; Pistone et al., 2021). These generate relative humidities exceeding 80% above 4 km when combined with the cooler high-altitude temperatures (Fig. 10a). Although there are two main aerosol plumes, the potential temperature profile is of a thermally stratified atmosphere containing many thinner well-mixed layer separated by discrete stability jumps (Fig. 10c), and the water vapor mixing ratio profile (Fig. 10c) also indicates there is only one truly well-mixed layer, capping the upper aerosol plume between 5.3-5.8 km with slackening winds. The lack of vertical mixing indicates the smoke plume heights are likely set above land. The upper-level aerosol plume registered both the highest OA:BC mass ratio and the highest SSA of the ORACLES-2016 campaign. More intense fires, with lower OA:BC are typically able to reach higher altitudes (Martin et al., 2010), but the higher OA:BC and NO_3:BC mass ratios aloft (Fig. 10b) may instead indicate more condensation of the emitted vapors aloft, aided by the cooler temperatures and higher relative humidities (Li et al., 2018).

Secondary aerosol formation is expected to proceed more quickly when $\frac{BC}{\Delta CO}$ ratios are lower (Vakkari et al., 2018), because the precursor gases may be more available (Yokelson et al., 2009). We first confirm that the flight's $\frac{BC}{\Delta CO}$ values remain statistically-similar as a function of *f44*: these remain within 7.5-7.9 $*10^{-3}$ independent of *f44* (Fig. 11a; see Figs. S9-S10 for the same analysis for the other flights). The corresponding OA:BC mass ratio decreases from 14.2 to 9.8 (Fig. 11b) - an

https://doi.org/10.5194/acp-2022-501
Preprint. Discussion started: 29 August 2022


Atmospheric Chemistry and Physics Discussions

approximate 35% decline in OA:BC over a span of 1-2 days. The corresponding SSA reduces from 0.89 to 0.865. The mean $AAE_{470-660}$ decreases from 1.25 to 1.21 ($\pm$0.07-0.08) as a function of the three *f44* bins, a statistically insignificant decline.

An evaluation of the changes to the particle size distribution with *f44*, normalized with respect to BC as a control for dilution, indicates the processes of condensation, coagulation - and volume loss consistent with the mass loss. As the aerosol ages chemically, the LDMA median diameter increases from $\sim$ 170 nm to $\sim$ 205 nm (Fig. 12a). BC particles are typically larger than OA particles (e.g., Fig. S6), and the reduction in the number of small particles indicates, besides coagulation of the OA particles upon the larger BC particles, also that most of the vapors are condensing on the larger BC particles, as opposed to forming new particles by nucleation. The total LDMA and CN particle number concentrations reduce from approximately 1200 cm^{-3} to 500 cm^{-3} with respect to BC, and 2400 cm^{-3} to 1500 cm^{-3}, respectively. The large difference in the two number concentrations likely reflects an instrument difference; both, however, indicate no net production of the smaller particles. The combined effect of condensation and coagulation results in an increase in the fraction of BC-containing particles (relative to LDMA numbers) from 0.18, to 0.23 and then 0.27 as *f44* increases. The evolution towards larger sizes would increase the SSA, all else equal. Instead, the SSA decreases in response to the decrease in OA, indicating again that changes in particle size do not dominate the SSA changes.

At the same time, the LDMA-determined particle volume decreases (Fig. 11b), indicating genuine particle mass loss that is consistent with the decrease in OA:BC. One mechanism for the mass loss could be evaporation through dilution. The selection for data samples with OA $>$ 20 μg m^{-3} focuses the analysis on the aerosol plume center, and a normalization by BC provides an additional control in Figs. 10a-d. A further assessment compared the CN particle number concentration to that from a CN heated to 150°C and found little difference (not shown, but consistent with Fig.S13). The heating can be interpreted as a proxy for dilution, as both physical processes increase volatility.

Another mechanism can be increasing oxidation through fragmentation, which can release higher-volatility particles that can then be removed through coagulation. Figs. 12c-d support that interpretation: both the LDMA and CN total particle number concentrations decrease with *f44*, consistent with processes occurring at the surface of the larger particles through diffusion - either coagulation or surface reactions. The oxidative environment, inferred from $\frac{O_3}{\Delta CO}$, remains constant with *f44* at a, indicating that these measures for oxidation have reached their upper limit. The reduction in the total non-BC aerosol mass, which reflects a reduction in the combined OA+NH_4+NO_3 mass but not SO_4 is nevertheless is in concert with the OA:BC decrease. The constancy of SO_4:BC confirms the aerosol age, as the lifetime of SO_2 is 1-2 days, after which its conversion to SO_4 will have ended. In summary we interpret Fig. 12 to reflect changes in the particle size distribution induced by condensation and coagulation, with little if any influence from dilution.

The backtrajectories do not show lower-level westerlies, in contrast to the *in-situ* profiles. We conjecture that the daytime aircraft sampling sampled a land breeze below 4 km that is converging above a warming continental surface and is not represented in the GFS meteorology. The ERA5 dataset, which has an hourly temporal resolution, might be able to address this hypothesis. Not shown, the marine boundary layer top is at one km, and did not include any BC, consistent with a slow entrainment time scale for aerosols (Diamond et al., 2018).

https://doi.org/10.5194/acp-2022-501
Preprint. Discussion started: 29 August 2022


Atmospheric Chemistry and Physics Discussions

A third mechanism for the loss of the overall particle mass can be through thermodynamics, consistent with the increase in NO_3:BC with altitude (Fig. **??**b). This mechanism is assessed in more detail within Section 7.

7 Does comparing to aerosol measured at Ascension Island indicate ongoing compositional changes?

A comparison to the aerosol properties measured at the more remote location of Ascension island by CLARIFY (Table 2) supports the process speculation that fragmentation of oxidized aerosol may be contributing to mass loss, by ultimately releasing some aerosol that can evaporation through photochemistry, similar to the younger aerosol sampled on 9/24/2016. Table 2 compares values for the aerosol parameters derived from the six ORACLES flights to the free-tropospheric values reported within Wu et al. (2020) and Taylor et al. (2020). The ORACLES 8/31/2017 flight also coincides with CLARIFY and occurred halfway to the island (Fig. 1). Important to this comparison, the $\frac{OA}{\Delta CO}$ values are comparable between the ORACLES-CLARIFY instruments on the intercomparison flight held on 18 August 2017, as are BC and SSA (Barrett et al., 2022). The similar $\frac{BC}{\Delta CO}$ ratios (Table 1) equal the maximum values inferred from the surface-based measurements at Ascension between June to October (Che et al., 2022). although these may also be subject to slight differences in methodology and are not shown in Table 2.

Overall, CLARIFY sampled more BC-enriched particles at Ascension in both number and mass, with slightly lower SSA, higher MAC_{660}s, and larger particle sizes. The OA:BC mass ratios are lower, because the OA masses themselves are much lower, typically < 4 μg m^{-3} (Wu et al., 2020). The H:C, O:C and OA:OC CLARIFY values (1.2-1.4, 0.7-0.8, 2.3) indicate slightly more oxidized aerosol at Ascension Wu et al. (2020) than for ORACLES, with the exception of 31 August 2017 (Fig. 5). Compared to the September ORACLES flights, the 8/31/2017 flight measured higher MACs, also a slightly lower OA:BC mass ratio - but here primarily because the BC mass is elevated (Fig. 3) -, larger median particle diameters, and a slightly lower SSA for the same BC number fraction (Fig. 8). The OA:BC mass ratios reduce by a factor of two between ORACLES and CLARIFY, primarily because the OA mass fractions reduce.

Although prior field campaigns that highlight a small net OA loss as BBA ages beyond a day (e.g., Capes et al., 2008; Jolleys et al., 2012, 2015; Hodzic et al., 2015; Konovalov et al., 2019; Farley et al., 2022), attributed to evaporation through dilution in Jolleys et al. (2012), the extent of the reduction - a factor of at least two - suggests a different process is dominant. Nevertheless, we examine if dilution could be factor, through comparing the number and volume size distributions measured by the TDMA at STP and at 150°C (Fig. S13); the heating is used as a proxy for dilution. Although the size distribution does not extend beyond 0.2 μm at most, missing the bulk of the aerosol mass, the size distributions change little between the temperatures, supporting the inference that evaporation through dilution does not explain differences in OA:BC between the two campaigns.

Another significant difference between ORACLES-2016 and CLARIFY is the inorganic nitrate (IN) fraction. Nitrate only contributes 10% to the total aerosol mass analyzed here, and only 8% of the total free-tropospheric aerosol mass during CLARIFY (Wu et al., 2020). The fraction that is inorganic nitrate is even smaller, but an examination of its fractional contribution may shed light on the evolution of southern African BBA. Interestingly, the 8/31/2017 inorganic nitrate fraction was 51% - intermediate to the ORACLES-2016 and CLARIFY values (Table 2). This suggests that organic nitrate becomes converted to inorganic nitrate as the aerosol ages. The air sampled during ORACLES was mildly acidic (Fig. S3), based on a simplification

https://doi.org/10.5194/acp-2022-501
Preprint. Discussion started: 29 August 2022


Atmospheric Chemistry and Physics Discussions

of the $NH_{4,measured}/NH_{4,predicted}$ relationship put forth in Zhang et al. (2007). A mild acidity will slow the rate of inorganic acid formation, and may help explain the lower IN fraction for ORACLES (20%-25%). Inorganic ammonium nitrate is held responsible for an increase in SSA with height at Ascension (Wu et al., 2020), as thermodynamic partitioning favors the particle phase at higher altitudes. The nitrate fraction is never large, and the coating on the BC will be dominated by OA by mass, so that the IN fraction may be more valuable as an indicator of ongoing oxidation that is also capable of increasing the MAC (Shrivastava et al., 2017). The sulfate fraction is similar between the two campaigns, including the 8/31/2017 flight, and seems unlikely to explain the differences in the MAC between the campaigns. Increasing coagulation of smaller particles upon the BC particles could help explain why the particle diameters are larger at Ascension compared to ORACLES-2016, at the same time that evaporation through photochemistry increases the fraction of BC-containing particles increase while decreasing the overall OA:BC mass ratio. It is also possible that the non-Lagrangian sampling is introducing a bias. We note that a more true Lagrangian analysis of filter samples finds aerosol volatility increases and continued OA loss during transport (Dang et al., 2022).

We also examine if a portion of the OA can thermodynamically repartition. We composite OA:BC, NO_3:BC and aerosol age by the free-tropospheric RH for all six flights to illuminate how much thermodynamical partitioning by altitude may be occurring. The higher altitudes in the free troposphere are also often more humid conditions (e.g., Fig 10, also shown more statistically in Adebiyi et al. (2015) and Pistone et al. (2021)). Physically-younger aerosol is more likely to occupy a more (relatively) humid, colder free troposphere at higher altitudes than is older aerosol (Fig. 10). The mean NO_3:BC ratio decreases by almost 50% as the free troposphere RH decreases from 70% to 30% (Fig. 13a), consistent with a thermodynamic repartitioning to the gas phase. The mean OA:BC mass ratio decreases from 10.5 $\pm$ 2.6 for RH = 60-80% to 9.9 $\pm$ 2.1 for 20% < RH < 40%. This indicates that a thermodynamical repartition can only explain a relative change in OA:BC of less than 10%. The winds that transport aerosol offshore also transport moisture, and the presence of moisture may also contribute to the OA mass loss, through increasing OH uptake and/or fragmentation (Li et al., 2018).

8 Discussion

An examination of the aerosol vertical structure and relationship to a chemical aging marker closer to the African continent indicates its increase in SSA with height can be explained primarily by more OA aloft. This contrasts with the attribution of the increase in SSA with height at Ascension to an increase in ammonium nitrate with height (Wu et al., 2020). At lower altitudes with slightly older aerosol, condensation and coagulation can increase the particle size, and evaporation through photochemistry can reduce the overall mass. Dilution is not thought to be as important as for northern hemisphere boreal fires, because the smoke distribution is so broad and loadings so large, composed of a homogeneization of many small continental small fires before the smoke is advected offshore.

A highlight of this study is its SSA_{530} best-fit regression on OA:BC: SSA_{530}=0.801+0.0055*(OA:BC). The range of OA:BC of 7 through 14 equates to an SSA variability of 0.83 to 0.89. This provides a straightforward connection between the BBA chemical and optical properties that is useful for the modeling of the direct aerosol radiative effect. Of course, use of such

https://doi.org/10.5194/acp-2022-501
Preprint. Discussion started: 29 August 2022


Atmospheric Chemistry and Physics Discussions

a best-fit is only effective if the model OA:BC mass ratios are realistic. Given that OA:BC mass ratios are often too low in models, their absorption of sunlight will also be overestimated (Brown et al., 2021). This study adds to literature indicating that OA model estimates made by multiplying the organic carbon by a factor of 1.4 will underestimate OA in this (and other) regions (Aiken et al., 2008; Tsigaridis et al., 2014; Shinozuka et al., 2020; Doherty et al., 2022). This study's OA:OC mass ratios of 2.2 ± 0.1 is also shown for the Atomic Tomography mission (Hodzic et al., 2020).

More sophisticated aerosol schemes can, in contrast, overestimate OA:BC mass ratios over the southeast Atlantic (Chylek et al., 2019), suggesting the loss of OA with aging or slower SOA production processes (Kroll and Seinfeld, 2008; McFiggans et al., 2019) may be under-accounted for. For the southeast Atlantic region, far removed from urban and industrial sources of pollution, continued production of SOA after 1-2 days is expected to remain minor (e.g., O'Brien and Kroll, 2019). This contrasts with northern hemisphere fire emission sources. Brown carbon production has been linked to low OA:BC ratios (Saleh et al., 2014; McClure et al., 2020), but this does not seem supported by the admittedly-limited ORACLES measurements of AAE and MAC, perhaps because brown carbon is typically more closely linked to primary than to secondary organic aerosol. Many prior studies find continuing oxidation of OA (see review by Shrivastava et al., 2017). This will be more important for remote environments containing thick smoke layers lacking additional pollution sources producing the precursor gases for additional SOA. Further work is needed to better support the process conclusion of this study, named that evaporation through photochemistry is the dominant chemical aging process over the southeast Atlantic, but nevertheless this study indicates the importance of developing sophisticated SOA schemes (e.g., Lou et al., 2020) for this regional climate.

September is unique in that meteorology and fire processes conspire to accentuate the direct radiative warming of the southeast Atlantic. August is more likely the peak burning month (Scholes et al., 1996), but the upper-level winds that transport the aerosol depend on a stronger heat low over southern Africa, and don't become well-established until September (Adebiyi and Zuidema, 2016; Kuete et al., 2020). The winds occur to the north of the heat low, and only dry convection lofts the aerosols to their altitude. The winds distribute aerosol as far away as south America (Holanda et al., 2020), so that the entire south Atlantic is covered by a blanket of highly-absorptive aerosol, with submicron BC mass fractions far exceeding the 2-10% estimated for western north America (Garofalo et al., 2019). The strong September upper-level winds also discourage subsidence (Chaboureau et al., 2022), and the cloud cover and height is affected more by meteorology than by aerosol during this month (Zhang and Zuidema, 2021). Less of the aerosol reaches the cloud top, reducing its entrainment (Zuidema et al., 2018; Shinozuka et al., 2020; Doherty et al., 2022) and ability to influence the cloud top inversion strength (Herbert et al., 2020). The net radiative impact will primarily be the direct aerosol radiative effect of the aerosol aloft then, lending further weight on model representation of SSA. Although IPPC AR5 assessments suggest the ability of smoke to both scatter and absorb sunlight leads to a net compensation globally, this will not be the case for the southeast Atlantic (Mallet et al., 2021).

Data availability. The data are available through doi=10.5067/Suborbital/ORACLES/P3/2016_V2 and doi=10.5067/Suborbital/ORACLES/P3/2017_V2

https://doi.org/10.5194/acp-2022-501
Preprint. Discussion started: 29 August 2022

Atmospheric Chemistry and Physics Discussions

Author contributions. The present work was conceived by P.Z., A. D., P.S. and S.H.. S.F. contributed to the HiGEAR data analysis, A.S. provided the BC datasets and P.S. the WRF-AAM model age estimates. Portions of this work first appeared in the M.S. thesis of A.D at U. of Hawaii. All authors contributed to the final writing.

Competing interests. Paquita Zuidema is a guest editor for the ACP Special Issue: "ACP special issue: New observations and related modelling studies of the aerosol–cloud–climate system in the Southeast Atlantic and southern Africa regions" The other authors declare no competing interests.

Acknowledgements. ORACLES is a NASA Earth Venture Suborbital-2 investigation, funded by the US National Aeronautics and Space Administration (NASA)'s Earth Sciences Division and managed through the Earth System Science Pathfinder Program Office (grant no. NNH13ZDA001N-EVS2). This work was further supported by the US Department of Energy grant DE-SC0018272 to P.Z. and P.S. and DE-SC0021250 to P.Z. We thank Hugh Coe, Huihiu Wu and Jonathan Taylor for interesting initial conversations that in particular encouraged us to examine the inorganic nitrate fraction.

https://doi.org/10.5194/acp-2022-501
Preprint. Discussion started: 29 August 2022

Atmospheric Chemistry and Physics Discussions

References

Adebiyi, A. A. and Zuidema, P.: The role of the southern African easterly jet in modifying the southeast Atlantic aerosol and cloud environments, Q. J. Roy. Meteor.Soc., 142, 1574–1589, https://doi.org/10.1002/qj.2765, 2016.

Adebiyi, A. A., Zuidema, P., and Abel, S. J.: The Convolution of Dynamics and Moisture with the Presence of Shortwave Absorbing Aerosols over the Southeast Atlantic, J. Climate, 28, 1997–2024, https://doi.org/10.1175/JCLI-D-14-00352.1, 2015.

Aiken, A. C., DeCarlo, P. F., and Jimenez, J. L.: Elemental analysis of organic species with electron ionization high-resolution mass spectrometry, Anal. Chem., 79, 8350–8358, 2007.

Aiken, A. C., DeCarlo, P. F., Kroll, J. H., Worsnop, D., Huffman, J. A., Docherty, K. S., Ulbrich, I., and et al., C. M.: O/C and OM/OC ratios of primary, secondary, and ambient organic aerosols with high-resolution time-of-flight aerosol mass spectrometry, Environ Sci Technol., 42, 4478–4485, 2008.

Akagi, S. K., Yokelson, R. J., Wiedinmyer, C., Alvarado, M. J., Reid, J. S., Karl, T., Crounse, J. D., and Wennberg, P. O.: Emission factors for open and domestic biomass burning for use in atmospheric models, Atmos. Chem. Phys., 11, 4039–4072, https://doi.org/10.5194/acp-11-4039-2011, 2011.

Andreae, M. O.: Emission of trace gases and aerosols from biomass burning – an updated assessment, Atmos. Chem. Phys., 19, 8523–8546, https://doi.org/10.5194/acp-19-8523-2019, 2019.

Baars, H., Radenz, M., Floutsi, A., Engelmann, R., Althausen, D., and et al., B. H.: Californian wildfire smoke over Europe: A first example of the aerosol observing capabilities of Aeolus compared to ground-based lidar, Geophy. Res. Lett., 48, https://doi.org/10.1029/2020GL092194, e2020GL092194, 2021.

Bahreini, R., Ervens, B., Middlebrook, A. M., Warneke, C., de Gouw, J. A., DeCarlo, P. F., and et al., J. L. J.: Organic aerosol formation in urban and industrial plumes near Houston and Dallas, Texas, J. Geophys. Res., 114, https://doi.org/10.1029/2008jd011493, 2009.

Barrett, P. A., Abel, S. J., Coe, H., Crawford, I., Dobracki, A., Haywood, J. M., Howell, S., Jones, A., Langridge, J., McFarquhar, G., Nott, G., Price, H., Redemann, J., Shinozuka, Y., Szpek, K., Taylor, J., Wood, R., Wu, H., Zuidema, P., Bauguitte, S., Bennett, R., Bower, K., Chen, H., Cochrane, S. P., Cotterell, M., Davies, N., Delene, D., Flynn, C., Freedman, A., Freitag, S., Gupta, S., Noone, D., Onasch, T. B., Podolske, J., Poellot, M. R., Schmidt, S. K., Springston, S., III, A. J. S., Trembath, J., Vance, A., Zawadowicz, M., and Zhang, J.: Intercomparison of airborne and surface-based measurements during the CLARIFY, ORACLES and LASIC field experiments, Atmos. Meas. Tech. Discuss., https://doi.org/10.5194/amt-2022-59, 2022.

Bond, T. C. and Bergstrom, R. W.: Light absorption by carbonaceous particles: an investigative review, Aer. Sci. Tech., 40, 27–67, https://doi.org/10.1080/02786820500421521, 2006.

Bond, T. C., Doherty, S. J., Fahey, D. W., Forster, P. M., Berntsen, T., DeAngelo, B. J., Flanner, M. G., Ghan, S., Kärcher, B., Koch, D., Kinne, S., and et al., Y. K.: Bounding the role of black carbon in the climate system: A scientific assessment, J. Geophys. Res., 118, 5380–5552, https://doi.org/10.1002/jgrd.50171, 2013.

Bowman, D. M., Balch, J. K., Artaxo, P., Bond, W. J., Carlson, J. M., Cochrane, M. A., D'Antonio, C. M., and et al., R. S. D.: Fire in the Earth System, Science, 324, 481–484, https://doi.org/10.1126/science.1163886, 2009.

Brown, H., Liu, X., Pokhrel, R., Murphy, S., Lu, Z., Saleh, R., Mielonen, T., Kokkola, H., Bergman, T., Myhre, G., Skeie, R. B., Watson-Paris, D., Stier, P., Johnson, B., Bellouin, N., Schulz, M., Vakkari, V., Beukes, J. P., vanZyl, P. G., Liu, S., and Chand, D.: Biomass burning aerosols in most climate models are too absobing, Nat. Comm., 12, 277, https://doi.org/10.1038/s41467-020-20482-9, 2021.

https://doi.org/10.5194/acp-2022-501
Preprint. Discussion started: 29 August 2022

Canagaratna, M. R., Jimenez, J. L., and et al., J. H. K.: Elemental ratio measurements of organic compounds using aerosol mass spectrometry: characterization, improved calibration, and implications, Atmos. Chem. Phys., 15, 253–272, https://doi.org/10.5194/acp-15-253-2015, 2015.

Capes, G., B.Johnson, McFiggans, G., Williams, P. I., Haywood, J., and Coe, H.: Aging of biomass burning aerosols over West Africa: Aircraft measurements of chemical composition, microphysical properties, and emission ratios, J. Geophys. Res., 113, https://doi.org/10.1029/2008jd009845, 2008.

Carter, T. S., Heald, C. L., Cappa, C. D., Kroll, J. H., Campos, T. L., Coe, H., Cotterel, M. I., Davies, N. W., Farmer, D. K., Fox, C., Garofalo, L. A., Hu, L., Langridge, J. M., Levin, E. J. T., Murphy, S. M., Pokhrel, R. P., Shen, Y., Szpek, K., Taylor, J. W., and Wu, H.: Investigating Carbonaceous Aerosol and its Absorption Properties from Fires in the western US (WE-CAN) and southern Africa (ORACLES and CLARIFY), J. Geophys. Res., 126, e2021JD034984, 2021.

Chaboureau, J.-P., Labbouz, L., Flamant, C., and Hodzic, A.: Acceleration of the southern African easterly jet driven by radiative effect of biomass burning aerosols and its impact on transport during AEROCLO-sA, Atmos. Chem. Phys. Discuss., https://doi.org/10.5194/acp-2022-233, 2022.

Che, H., Segal-Rozenhaimer, M., Zhang, L., Dang, C., Zuidema, P., III, A. J. S., Zhang, X., and Flynn, C.: Seasonal variations in fire conditions are important drivers to the trend of aerosol optical properties over the south-eastern Atlantic, Atmos. Chem. Phys. Discuss., 22, https://doi.org/10.5194/acp-2022-160, 2022.

Christian, T. J., Kleiss, B., Yokelson, R. J., Holzinger, R., Crutzen, P. J., Hao, W. M., Saharjo, B. H., and Ward, D. E.: Comprehensive laboratory measurements of biomass-burning emissions: 1. Emissions from Indonesian, African, and other fuels, J. Geophys. Res., 108, 4719, https://doi.org/10.1029/2003JD003704, 2003.

Chylek, P., Lee, J. E., Romonosky, D. E., Gallo, F., Lou, S., and et al., M. S.: Mie Scattering Captures Observed Optical Properties of Ambient Biomass Burning Plumes Assuming Uniform Black, Brown, and Organic Carbon Mixtures, J. Geophys. Res., 124, 11 406–11 427, https://doi.org/10.1029/2019jd031224, 2019.

Collier, S., Zhou, S., Onasch, T. B., Jaffe, D. A., Kleinman, L., A. J. Sedlacek, I., Briggs, N. L., Hee, J., Fortner, E., and et al., J. E. S.: Regional Influence of Aerosol Emissions from Wildfires Driven by Combustion Efficiency: Insights from the BBOP Campaign, Environ Sci Technol., 50, 8613–8622, https://doi.org/10.1021/acs.est.6b01617, 2016.

Cubison, M. J., Ortega, A. M., Hayes, P. L., Farmer, D. K., Day, D., Lechner, M. J., Brune, W. H., Apel, E., and et al., D.: Effects of aging on organic aerosol from open biomass burning smoke in aircraft and laboratory studies, Atmos. Chem. Phys., 11, 12 049–12 064, https://doi.org/10.5194/acp-11-12049-2011, 2011.

Dang, C., Segal-Rozenhaimer, M., Che, H., Zhang, L., Formenti, P., Taylor, J., Dobracki, A., Purdue, S., Wong, P.-S., Nenes, A., Sedlacek, A., Coe, H., Redemann, J., Zuidema, P., and Haywood, J.: Biomass burning and marine aerosol processing over the southeast Atlantic Ocean: A TEM single particle analysis, Atmos. Chem. Phys., https://doi.org/10.5194/acp-2021-724, 2022.

Darmenov, A. and da Silva, A.: The Quick Fire Emissions Dataset (QFED) - Documentation of Versions 2.1, 2.2, and 2.4, 32, 2013.

Davies, N. W., Fox, C., Szpek, K., Cotterell, M. I., Taylor, J. W., Allan, J. D., Williams, P. I., Trembath, J., Haywood, J. M., and Langridge, J. M.: Evaluating biases in filter-based aerosol absorption measurements using photoacoustic spectroscopy, Atmos. Meas. Tech., 12, 3417–3434, https://doi.org/10.5194/amt-12-3417-2019, 2019.

de Graaf, M., Schulte, R., Peers, F., Waquet, F., Tilstra, L. G., and Stammes, P.: Comparison of south-east Atlantic aerosol direct radiative effect over clouds from SCIAMACHY, POLDER and OMI–MODIS, Atmos. Chem. Phys., 20, 6707–6723, https://doi.org/10.5194/acp-20-6707-2020, 2020.

https://doi.org/10.5194/acp-2022-501
Preprint. Discussion started: 29 August 2022

Denjean, C., Bourrianne, T., Burnet, F., Mallet, M., Maury, N., Colomb, A., Dominutti, P., Brito, J., Dupuy, R., Sellegri, K., Schwarzenboeck, A., Flamant, C., and Knippertz, P.: Overview of aerosol optical properties over southern West Africa from DACCIWA aircraft measurements, Atmos. Chem. Phys., 20, 4735–4756, https://doi.org/10.5194/acp-20-4735-2020, 2020a.

Denjean, C., Brito, J., Libois, Q., Mallet, M., Bourrianne, T., and et al., F. B.: Unexpected Biomass Burning Aerosol Absorption Enhancement Explained by Black Carbon Mixing State, Geophys. Res. Lett., 47, https://doi.org/10.1029/2020gl089055, 2020b.

Diamond, M. S., Dobracki, A., Freitag, S., Small Griswold, J. D., Heikkila, A., Howell, S. G., Kacarab, M. E., Podolske, J. R., Saide, P. E., and Wood, R.: Time-dependent entrainment of smoke presents an observational challenge for assessing aerosol–cloud interactions over the southeast Atlantic Ocean, Atmos. Chem. Phys., 18, 14 623–14 636, https://doi.org/10.5194/acp-18-14623-2018, 2018.

Dobracki, A., Zuidema, P., Howell, S., Saide, P., Freitag, S., Aiken, A. C., Burton, S. P., III, A. J. S., Redemann, J., and Wood, R.: Nonreversible aging can increase solar absorption in African biomass burning aerosol plumes of intermediate age, Atmos. Chem. Phys. Discuss., https://doi.org/10.5194/acp-2021-1081, preprint, 2022.

Doherty, S. J., Saide, P., Zuidema, P., Shinozuka, Y., Ferrada, G., and et al., H. G.: Modeled and observed properties related to the direct aerosol radiative effect of biomass burning aerosol over the Southeast Atlantic, Atmos. Chem. Phys., 22, 1,46, https://doi.org/10.5194/acp-22-1-2022, 2022.

Dubovik, O., Holben, B. N., Eck, T. F., Smirnov, A., Kaufman, Y. J., King, M. D., Tanre, D., and Slutsker, I.: Variability of absorption and optical properties of key aerosol types observed in worldwide locations, J. Atmos. Sci., 59, 590–608, 2002.

Eck, T. F., Holben, B. N., Reid, J. S., Mukelabai, M. M., Piketh, S. J., and et al., O. T.: A seasonal trend of single scattering albedo in southern African biomass-burning particles: Implications for satellite products and estimates of emissions for the world's largest biomass-burning source, J. Geophys. Res., 118, https://doi.org/10.1002/jgrd.50500, 2013.

Farley, R., Bernays, N., Jaffe, D. A., Ketcherside, D., Hu, L., Zhou, S., Collier, S., and Zhang, Q.: Persistent influence of wildfire emissions in the western United States and characteristics of aged biomass burning organic aerosols under clean air conditios, Env. Sci. Tech., 56, 3645–3657, https://doi.org/10.1021/acs.est.1c07301, 2022.

Farmer, D., Matsunaga, A., Docherty, K. S., Surratt, J. D., Seinfeld, J. H., Ziemann, P. J., and Jimenez, J. L.: Response of an aerosol mass spectrometer to organonitrates and organosulfates and implications for atmospheric chemistry, Proc Natl Acad Sci USA, 107, 6670–6675, https://doi.org/10.1073/pnas.0912340107, 2011.

Formenti, P., Elbert, W., Maenhaut, W., Haywood, J., Osborne, S., and Andreae, M. O.: Inorganic and carbonaceous aerosols during the Southern African Regional Science Initiative (SAFARI 2000) experiment: Chemical characteristics, physical properties, and emission data for smoke from African biomass burning, J. Geophys. Res., 108, https://doi.org/10.1029/2002JD002408, 2003.

Garofalo, L. A., Pothier, M. A., Levin, E. J., Campos, T., Kreidenweis, S. M., and Farmer, D. K.: Emission and Evolution of Submicron Organic Aerosol in Smoke from Wildfires in the Western United States, ACS Earth Space Chem., 3, 1237–1247, https://doi.org/10.1021/acsearthspacechem.9b00125, 2019.

George, I. J. and Abbatt, J. P. D.: Chemical evolution of secondary organic aerosol from OH-initiated heterogeneous oxidation, Atmos. Chem. Phys., 10, 5551–5563, https://doi.org/10.5194/acp-10-5551-2010, 2010.

Giglio, L., van der Werf, G. R., Randerson, J. T., Collatz, G., and Kasibhatla, P.: Global estimation of burned area using MODIS active fire observations, Atmos. Chem. Phys., 6, 957–974, https://doi.org/10.5194/acp-6-957-2006, 2006.

Graaf, M. D., Bellouin, N., Tilstra, L. G., Haywood, J., and Stammes, P.: Aerosol direct radiative effect of smoke over clouds over the southeast Atlantic Ocean from 2006 to 2009, Geophys. Res. Lett., 41, 7723–7730, https://doi.org/10.1002/2014GL061103, 2014.

https://doi.org/10.5194/acp-2022-501
Preprint. Discussion started: 29 August 2022

Atmospheric Chemistry and Physics Discussions

Gysel, M., Laborde, M., Olfert, J. S., Subramanian, R., and Gröhn, A.: Effective density of Aquadag and fullerene soot black carbon reference materials used for SP2 calibration, Atmos. Meas. Tech. Disc., 4, 4937–4955, https://doi.org/10.5194/amtd-4-4937-2011, 2011.

Haywood, J. M., Osborne, S. R., Francis, P. N., Keil, A., Andreae, P. F. M. O., and Kaye, P. H.: The mean physical and optical properties of regional haze dominated by biomass burning aerosol measured from the C-130 aircraft during SAFARI 2000, J. Geophys. Res., 108, 8473–8481, https://doi.org/10.1029/2002JD002226, 2003.

Haywood, J. M., Abel, S. J., Barrett, P. A., Bellouin, N., Blyth, A., Bower, K. N., Brooks, M., Carslaw, K., Che, H., Coe, H., Cotterell, M. I., Crawford, I., Cui, Z., Davies, N., Dingley, B., Field, P., Formenti, P., Gordon, H., de Graaf, M., Herbert, R., Johnson, B., Jones, A. C., Langridge, J. M., Malavelle, F., Partridge, D. G., Peers, F., Redemann, J., Stier, P., Szpek, K., Taylor, J. W., Watson-Parris, D., Wood, R., Wu, H., and Zuidema, P.: Overview: The CLoud-Aerosol-Radiation Interaction and Forcing: Year-2017 (CLARIFY-2017) measurement campaign, Atmos. Chem. Phys., 21, 1049–1084, https://doi.org/10.5194/acp-21-1049-2021, 2021.

Heald, C. L., Kroll, J. H., Jimenez, J. L., Docherty, K. S., DeCarlo, P. F., Aiken, A. C., Chen, Q., Martin, S. T., Farmer, D. K., and Artaxo, P.: A simplified description of the evolution of organic aerosol composition in the atmosphere, Geophys. Res. Lett., 37, https://doi.org/10.1029/2010gl042737, 2010.

Herbert, R. J., Bellouin, N., Highwood, E. J., and Hill, A. A.: Diurnal cycle of the semi-direct effect from a persistent 1300 absorbing aerosol layer over marine stratocumulus in large-eddy simulations, Atmos. Chem. Phys., 20, 1317–1340, https://doi.org/10.5194/acp-20-1317-2020, 2020.

Hodshire, A. L., Akherati, A., Alvarado, M., Brown-Steiner, B., Jathar, S., Jimenez, J. L., Kreidenweis, S., Lonsdale, C., Onasch, T., Ortega, A., and Pierce, J.: Aging Effects on Biomass Burning Aerosol Mass and Composition: A Critical Review of Field and Laboratory Studies, Environ Sci Technol, 53, 10 007–10 022, https://doi.org/10.1021/acs.est.9b02588, 2019.

Hodshire, A. L., Ramnarine, E., Akherati, A., Alvarado, M. L., Farmer, D. K., Jathar, S. H., and et al., S. M. K.: Dilution impacts on smoke aging: evidence in Biomass Burning Observation Project (BBOP) data, Atmos. Chem. Phys., 21, 6839–6855, https://doi.org/10.5194/acp-21-6839-2021, 2021.

Hodzic, A., Madronich, S., Kasibhatla, P. S., Tyndall, G., Aumont, B., Jimenez, J. L., Lee-Taylor, J., and Orlando, J.: Organic photolysis reactions in tropospheric aerosols: effect on secondary organic aerosol formation and lifetime, Atmos. Chem. Phys., 15, 9253–9269, https://doi.org/10.5194/acp-15-9253-2015, 2015.

Hodzic, A., Campuzano-Jost, P., Bian, H., Chin, M., Colarco, P. R., Day, D. A., Froyd, K. D., Heinold, B., and et al., D. S. J.: Characterization of organic aerosol across the global remote troposphere: a comparison of ATom measurements and global chemistry models, Atmos. Chem. Phys., 20, 4607–4635, https://doi.org/10.5194/acp-20-4607-2020, 2020.

Holanda, B. A., Pöhlker, M. L., Walter, D., Saturno, J., Sörgel, M., Ditas, J., Ditas, F., Schulz, C., Franco, M. A., Wang, Q., Donth, T., Artaxo, P., Barbosa, H. M. J., Borrmann, S., Braga, R., Brito, J., Cheng, Y., Dollner, M., Kaiser, J. W., Klimach, T., Knote, C., Krüger, O. O., Fütterer, D., Lavrič, J. V., Ma, N., Machado, L. A. T., Ming, J., Morais, F. G., Paulsen, H., Sauer, D., Schlager, H., Schneider, J., Su, H., Weinzierl, B., Walser, A., Wendisch, M., Ziereis, H., Zöger, M., Pöschl, U., Andreae, M. O., and Pöhlker, C.: Influx of African biomass burning aerosol during the Amazonian dry season through layered transatlantic transport of black carbon-rich smoke, Atmos. Chem. Phys., 20, 4757–4785, https://doi.org/10.5194/acp-20-4757-2020, 2020.

Holder, A. L., Hagler, G. S., Aurell, J., Hays, M. D., and Gullett, B. K.: Particulate matter and black carbon optical properties and emission factors from prescribed fires in the southeastern United States, J. Geophys. Res., 121, 3465–3483, https://doi.org/10.1002/2015JD024321, 2016.

https://doi.org/10.5194/acp-2022-501
Preprint. Discussion started: 29 August 2022

Atmospheric Chemistry and Physics Discussions

Howell, S. G., Clarke, A. D., Freitag, S., McNaughton, C. S., Kapustin, V., Brekovskikh, V., Jimenez, J.-L., and Cubison, M. J.: An airborne assessment of atmospheric particulate emissions from the processing of Athabasca oil sands, Atmos. Chem. Phys., 14, 5073–5087, https://doi.org/10.5194/acp-14-5073-2014, 2014.

Howell, S. G., Freitag, S., Dobracki, A., Smirnow, N., and III, A. J. S.: Undersizing of aged African biomass burning aerosol by an ultra-high-sensitivity aerosol spectrometer, Atmos. Meas. Tech., 14, 7381–7404, https://doi.org/10.5194/amt-14-7381-2021, 2021.

Huntley, B. J.: Angola in outline: physiography, climate and patters of biodiversity, chap. 2, pp. 15–42, Springer, https://doi.org/10.1007/978-3-030-03083-4, 2019.

Janhäll, S., Andreae, M. O., and Pöschl, U.: Biomass burning aerosol emissions from vegetation fires: particle number and mass emission factors and size distributions, Atmos. Chem. Phys., 10, 1427–1439, 2010.

Jimenez, J. L., Canagaratna, M. R., Donahue, N. M., Prevot, A. S. H., Zhang, Q., Kroll, J. H., DeCarlo, P. F., and al., J. D. A.: Evolution of organic aerosols in the atmosphere, Science, 326, 1525–1529, https://doi.org/10.1126/science.1180353, 2009.

Jolleys, M. D., Coe, H., McFiggans, G., Capes, G., Allan, J. D., Crosier, J., Williams, P. I., Allen, G., Bower, K. N., Jimenez, J. L., Russell, L. M., Grutter, M., and Baumgardner, D.: Characterizing the aging of biomass burning organic aerosol by use of mixing ratios: a meta-analysis of four regions, Environ. Sci. Technol., 46, 13 093–13 102, 2012.

Jolleys, M. D., Coe, H., McFiggans, G., Taylor, J. W., O'Shea, S. J., Breton, M. L., Bauguitte, S. J.-B., Moller, S., and et al., P. D. C.: Properties and evolution of biomass burning organic aerosol from Canadian boreal forest fires, Atmos. Chem. Phys., 15, 3077–3095, https://doi.org/10.5194/acp-15-3077-2015, 2015.

Keil, A. and Haywood, J. M.: Solar radiative forcing by biomass burning aerosol particles during SAFARI 2000: A case study based on measured aerosol and cloud properties, J. Geophys. Res., 108, https://doi.org/10.1029/2002JD002315, 2003.

Kondo, Y., Matsui, H., Moteki, N., Sahu, L., Takegawa, N., Kajino, M., Zhao, Y., Cubison, M. J., Jimenez, J. L., Vay, S., Diskin, G. S., Anderson, B., Wisthaler, A., Mikoviny, T., Fuelberg, H. E., Blake, D. R., Huey, G., Weinheimer, A. J., Knapp, D. J., and Brune, W. H.: Emissions of black carbon, organic, and inorganic aerosols from biomass burning in North America and Asia in 2008, J. Geophys. Res., 116, 2011.

Konovalov, I. B., Beekmann, M., Golovushkin, N. A., and Andreae, M. O.: Nonlinear behavior of organic aerosol in biomass burning plumes: a microphysical model analysis, Atmos. Chem. Phys., 19, 12 091–12 119, https://doi.org/10.5194/acp-19-12091-2019, 2019.

Korontzi, S., Ward, D. E., Susott, R. A., Yokelson, R. J., Justice, C. O., Hobbs, P. V., Smithwick, E. A. H., and Hao, W. M.: Seasonal variation and ecosystem dependence of emission factors for selected trace gases and PM2.5 for southern African savanna fires, J. Geophys. Res., 108, https://doi.org/10.1029/2003JD003730, 2003.

Kroll, J., Smith, J. D., Che, D. L., Kessler, S. H., Worsnop, D. R., and Wilson, K. R.: Measurement of fragmentation and functionalization pathways in the heterogeneous oxidation of oxidized organic aerosol, Phys. Chem. Chem. Phys., 11, 8005–8014, https://doi.org/10.1039/B905289E, 2009.

Kroll, J. H. and Seinfeld, J. H.: Chemistry of secondary organic aerosol: Formation and evolution of low-volatility organics in the atmosphere, Atmos. Env., 42, 3593–3624, 2008.

Kroll, J. H., Donahue, N. M., Jimenez, J. L., Kessler, S. H., Canagaratna, M. R., Wilson, K. R., and et al., K. E. A.: Carbon oxidation state as a metric for describing the chemistry of atmospheric organic aerosol, Nat Chem., 3, 133–139, https://doi.org/10.1038/nchem.948, 2011.

Kuete, G., Mba, W. P., and Washington, R.: African Easterly Jet South: control, maintenance mechanisms and link with Southern subtropical waves, Clim Dyn., 54, 1539–1552, https://doi.org/10.1007/s00382-019-05072-w, 2020.

https://doi.org/10.5194/acp-2022-501
Preprint. Discussion started: 29 August 2022

Laborde, M., Schnaiter, M., Linke, C., Saathoff, H., Naumann, K., Mohler, O., Berlenz, S., Wagner, U., Taylor, J., Liu, D., Flynn, M., Allan, J., Coe, H., Heimerl, K., Dahlkotter, F., Weinzierl, B., Wollny, A., Zanatta, M., Cozic, J., Laj, P., Hitzenberger, R., Schwarz, J., and Gysel, M.: Single Particle Soot Photometer intercomparison at the AIDA chamber, Atmos. Meas. Tech., 5, 3077–3097, https://doi.org/10.5194/amt-5-3077-2012, 2012.

Laskin, A., Laskin, J., and Nizkorodov, S. A.: Chemistry of atmospheric brown carbon, Chem. Rev., 155, 4335–4382, https://doi.org/10.1021/cr5006167, 2015.

Li, Z., Smith, K. A., and Cappa, C. D.: Influence of relative humidity on the heterogeneous oxidation of secondary organic aerosol, Atmos. Chem. Phys., 18, 14 585–14 608, https://doi.org/10.5194/acp-18-14585-2018, 2018.

Lou, S., Shrivastava, M., Easter, R. C., Yang, Y., Ma, P.-L., Wang, H., Cubison, M., Campuzano-Jost, P., and et al., J. L. J.: New SOA Treatments Within the Energy Exascale Earth System Model (E3SM): Strong Production and Sinks Govern Atmospheric SOA Distributions and Radiative Forcing, J. Adv. Mod. Earth Sys., 12, https://doi.org/10.1029/2020ms002266, 2020.

Mallet, M., Solmon, F., Nabat, P., Elguindi, N., Waquet, F., and et al., D. B.: Direct and semi-direct radiative forcing of biomass-burning aerosols over the southeast Atlantic (SEA) and its sensitivity to absorbing properties: a regional climate modeling study, Atmos. Chem. Phys., 20, 13 191–13 216, https://doi.org/10.5194/acp-20-13191-2020, 2020.

Mallet, M., Nabat, P., Johnson, B., Michou, M., Haywood, J. M., Chen, C., and Dubovik, O.: Climate models generally underrepresent the warming by Central Africa biomass-burning aerosols over the Southeast Atlantic, Sci. Adv., 7, eabg9998, https://doi.org/10.1126/sciadv.abg9998, 2021.

Martin, M. V., Logan, J. A., Kahn, R. A., Leung, F.-Y., Nelson, D. L., and Diner, D. J.: Smoke injection heights from fires in North America: Analysis of 5 years of satellite observations, Atmos. Chem. Phys., 10, 1491–1510, https://doi.org/10.5194/acp-10-1491-2010, 2010.

McClure, C. D., Lim, C. Y., Hagan, D. H., Kroll, J., and Cappa, C.: Biomass-burning-derived particles from a wide variety of fuels – Part 1: Properties of primary particles, Atmos. Chem. Phys., 20, 1531–1547, https://doi.org/10.5194/acp-20-1531-2020, 2020.

McFiggans, G., Mentel, T. F., and Wildt, J.: Secondary organic aerosol reduced by mixture of atmospheric vapours, Nature, 565, 587–593, https://doi.org/10.1038/s41586-018-0871-y, 2019.

Myhre, G., Samset, B. H., Schulz, M., Balkanski, Y., Bauer, S., and et al., T. K. B.: Radiative forcing of the direct aerosol effect from AeroCom Phase II simulations, Atmospheric Chemistry and Physics, 13, 1853–1877, https://doi.org/10.5194/acp-13-1853-2013, 2013.

Ng, N. L., Canagaratna, M. R., Zhang, Q., Jimenez, J. L., Tian, J., and et al., U.: Organic aerosol components observed in Northern Hemispheric datasets from Aerosol Mass Spectrometry, Atmos. Chem. Phys., 10, 4625–4641, https://doi.org/10.5194/acp-10-4625-2010, 2010.

Ng, N. L., Canagaratna, M. R., Jimenez, J. L., Chhabra, P. S., Seinfeld, J. H., and Worsnop, D. R.: Changes in organic aerosol composition with aging inferred from aerosol mass spectra, Atmos. Chem. Phys., 11, 6465–6474, https://doi.org/10.5194/acp-11-6465-2011, 2011.

Nicholson, S. E. and Grist, J. P.: The seasonal evolution of the atmospheric circulation over West Africa and equatorial Africa, J. Clim., 16, 1013–1030, 2003.

O'Brien, R. E. and Kroll, J. H.: Photolytic Aging of Secondary Organic Aerosol: Evidence for a Substantial Photo-Recalcitrant Fraction, J. Phys. Chem. Lett., 10, 4003–4009, https://doi.org/10.1021/acs.jpclett.9b01417, 2019.

Pendergrass, A. G. and Hartmann, D. L.: Global-mean precipitation and black carbon in AR4 simulations, Geophys. Res. Lett., 39, https://doi.org/10.1029/2011GL050067, l01703, 2012.

Pistone, K., Redemann, J., Doherty, S., Zuidema, P., Burton, S., Cairns, B., Cochrane, S., Ferrare, R., Flynn, C., Freitag, S., Howell, S., Kacenelenbogen, M., LeBlanc, S., Liu, X., Schmidt, K. S., Sedlacek III, A. J., Segal-Rosenhaimer, M., Shinozuka, Y., Stamnes, S., van

Diedenhoven, B., Van Harten, G., and Xu, F.: Intercomparison of biomass burning aerosol optical properties from in-situ and remote-sensing instruments in ORACLES-2016, Atmos. Chem. Phys., 19, 9181–9208, https://doi.org/10.5194/acp-19-9181-2019, 2019.

Pistone, K., Zuidema, P., Wood, R., Diamond, M., da Silva, A. M., Ferrada, G., Saide, P., Ueyama, R., Pfister, J.-M. R. L., Podolske, J., Noone, D., Bennett, R., Stith, E., Carmichael, G., Redemann, J., Flynn, C., LeBlanc, S., Segal-Rozenhaimer, M., and Shinozuka, Y.: Exploring the elevated water vapor signal associated with the free-tropospheric biomass burning plume over the southeast Atlantic Ocean, Atmos. Chem. Phys., 21, 9643–9668, https://doi.org/10.5194/acp-21-9643-2021, 2021.

Pokhrel, R. P., Gordon, J., Fiddler, M., and Bililign, S.: Determination of emission factors of pollutants from biomass burning of African fuels in laboratory measurements, J. Geophys. Res., 126, https://doi.org/10.1029/2021JD034731, e2021JD034731, 2021.

Ramo, R., Roteta, E., Bistinas, I., van Wees, D., Bastarrika, A., Chuvieco, E., and der Werf, G. R.: African burned area and fire carbon emissions are strongly impacted by small fires undetected by coarse resolution satellite data, Proc. Nat. Ac. Sci., 118, e2011160 118, https://doi.org/10.1073/pnas.2011160118, 2021.

Redemann, J., Russell, P. B., and Hamill, P.: Dependence of aerosol light absorption and single-scattering albedo on ambient relative humidity for sulfate aerosols with black carbon cores, J. Geophys. Res., 106, 27 485–27 495, 2001.

Redemann, J., Wood, R., Zuidema, P., Doherty, S. J., Luna, B., LeBlanc, S. E., Diamond, M. S., Shinozuka, Y., Chang, I. Y., Ueyama, R., Pfister, L., Ryoo, J.-M., Dobracki, A. N., da Silva, A. M., Longo, K. M., Kacenelenbogen, M. S., Flynn, C. J., Pistone, K., Knox, N. M., Piketh, S. J., Haywood, J. M., Formenti, P., Mallet, M., Stier, P., Ackerman, A. S., Bauer, S. E., Fridlind, A. M., Carmichael, G. R., Saide, P. E., Ferrada, G. A., Howell, S. G., Freitag, S., Cairns, B., Holben, B. N., Knobelspiesse, K. D., Tanelli, S., L'Ecuyer, T. S., Dzambo, A. M., Sy, O. O., McFarquhar, G. M., Poellot, M. R., Gupta, S., O'Brien, J. R., Nenes, A., Kacarab, M., Wong, J. P. S., Small-Griswold, J. D., Thornhill, K. L., Noone, D., Podolske, J. R., Schmidt, K. S., Pilewskie, P., Chen, H., Cochrane, S. P., Sedlacek, A. J., Lang, T. J., Stith, E., Segal-Rozenhaimer, M., Ferrare, R. A., Burton, S. P., Hostetler, C. A., Diner, D. J., Seidel, F. C., Platnick, S. E., Myers, J. S., Meyer, K. G., Spangenberg, D. A., Maring, H., and Gao, L.: An overview of the ORACLES (ObseRvations of Aerosols above CLouds and their intEractionS) project: aerosol–cloud–radiation interactions in the southeast Atlantic basin, Atmos. Chem. Phys., 21, 1507–1563, https://doi.org/10.5194/acp-21-1507-2021, 2021.

Ryoo, J.-M., Pfister, L., Ueyama, R., Zuidema, P., Wood, R., Chang, I., and Redemann, J.: A meteorological overview of the ORACLES (ObseRvations of Aerosols above CLouds and their intEractionS) campaign over the southeast Atlantic during 2016–2018: Part 1 - Climatology, Atmos. Chem. Phys., 21, 16 689–16 707, https://doi.org/10.5194/acp-21-16689-2021, 2021.

Ryoo, J.-M., Pfister, L., Ueyama, R., Zuidema, P., Wood, R., Chang, I., and Redemann, J.: A meteorological overview of the ORACLES (ObseRvations of Aerosols above CLouds and their intEractionS) campaign over the southeast Atlantic during 2016–2018: Part 1 - Daily and Synoptic Characteristics, Atmos. Chem. Phys. Disc., 22, https://doi.org/10.5194/acp-2022-256, 2022.

Saide, P., Thompson, G., Eidhammer, T., da Silva, A. M., and Carmichael, R. B. P. G. R.: Assessment of biomass burning smoke influence on environmental conditions for multi-year tornado outbreaks by combining aerosol-aware microphysics and fire emission constraints, J Geophys. Res., 121, 10 294–10 311, https://doi.org/10.1002/2016JD025056, 2016.

Saleh, R., Robinson, E., and et al., D. T.: Brownness of organics in aerosols from biomass burning linked to their black carbon content, Nature Geosci., 7, 647–650, https://doi.org/10.1038/ngeo2220, 2014.

Scholes, R. J., Ward, D. E., and Justice, C. O.: Emissions of trace gases and aerosol particles due to vegetation burning in southern hemisphere Africa, J. Geophys. Res., 101, 23 677–23 682, https://doi.org/10.1029/95JD02049, 1996.

https://doi.org/10.5194/acp-2022-501
Preprint. Discussion started: 29 August 2022

Atmospheric Chemistry and Physics Discussions

Shank, L. M., Howell, S., Clarke, A. D., Freitag, S., Brekhovskikh, V., Kapustin, V., McNaughton, C., Campos, T., and Wood, R.: Organic matter and non-refractory aerosol over the remote Southeast Pacific: oceanic and combustion sources, Atmos. Chem. Phys., 12, 557–576, https://doi.org/10.5194/acp-12-557-2012, 2012.

Shea, R. W., Shea, B. W., Kauffman, J. B., Ward, D. E., Haskins, C. I., and Scholes, M. C.: Fuel biomass and combustion factors associated with fires in savanna ecosystems of South Africa and Zambia, J. Geophys. Res., 101, 23,551– 23,568, 1996.

Shinozuka, Y., Saide, P. E., Ferrada, G. A., Burton, S. P., Ferrare, R., Doherty, S. J., Gordon, H., Longo, K., Mallet, M., Feng, Y., Wang, Q., Cheng, Y., Dobracki, A., Freitag, S., Howell, S. G., LeBlanc, S., Flynn, C., Segal-Rosenhaimer, M., Pistone, K., Podolske, J. R., Stith, E. J., Bennett, J. R., Carmichael, G. R., da Silva, A., Govindaraju, R., Leung, R., Zhang, Y., Pfister, L., Ryoo, J.-M., Redemann, J., Wood, R., and Zuidema, P.: Modeling the smoky troposphere of the southeast Atlantic: a comparison to ORACLES airborne observations from September of 2016, Atmos. Chem. Phys., 20, 11,491–11,526, https://doi.org/10.5194/acp-20-11491-2020, 2020.

Shrivastava, M., Cappa, C. D., Fan, J., Goldstein, A. H., Guenther, A., Jimenez, J. L., and et al., C. K.: Recent advances in understanding secondary organic aerosol: Implications for global climate forcing, Rev. Geophys., 55, 509–559, https://doi.org/10.1002/2016RG000540, 2017.

Solmon, F., Elguindi, N., and et al., M. M.: West African monsoon precipitation impacted by the South Eastern Atlantic biomass burning aerosol outflow, npj Clim Atmos Sci., 4, https://doi.org/10.1038/s41612-021-00210-w, 2021.

Stein, A. F., Draxler, R. R., Rolph, G. D., Stunder, B. J. B., Cohen, M. D., and Ngan, F.: NOAA's HYSPLIT Atmospheric Transport and Dispersion Modeling System, Bull. Am. Meteor. Soc., 96, 2059–2077, https://doi.org/10.1175/BAMS-D-14-00110.1, 2015.

Taylor, J. W., Wu, H., Szpek, K., Bower, K., Crawford, I., Flynn, M. J., Williams, P. I., Dorsey, J., Langridge, J. M., and et al.: Absorption closure in highly aged biomass burning smoke, Atmos. Chem. Phys., 20, 11 201–11 221, https://doi.org/10.5194/acp-20-11201-2020, 2020.

Thompson, G. and Eidhammer, T.: A study of aerosol impacts on clouds and precipitation development in a large winter cyclone, J. Atmos. Sci., 71, 3636–3658, https://doi.org/10.1175/JAS-D-13-0305.1, 2014.

Tsigaridis, K., Daskalakis, N., Kanakidou, M., Adams, P. J., Artaxo, P., Bahadur, R., Balkanski, Y., Bauer, S. E., Bellouin, N., and Benedetti, A. e. a.: The AeroCom evaluation and intercomparison of organic aerosol in global models, Atmos. Chem. Phys., 14, 10 845–10 895, https://doi.org/10.5194/acp-14-10845-2014, 2014.

Vakkari, V., Beukes, J. P., Maso, M. D., Aurela, M., Josipovic, M., and van Zyl, P. G.: Major secondary aerosol formation in southern African open biomass burning plumes, Nature Geo., 11, 580–583, https://doi.org/10.1038/s41561-018-0170-0, 2018.

van der Werf, G. R., Randerson, J. T., Giglio, L., Collatz, G. J., Mu, M., Kasibhatla, P. S., and Morton, D. C. e. a.: Global fire emissions and the contribution of deforestation, savanna, forest, agricultural, and peat fires (1997–2009), Atmos. Chem. Phys., 10, 11 707–11 735, https://doi.org/10.5194/acp-10-11707-2010, 2010.

vanKrevelen, D. W.: Graphical-statistical method for the study of structure and reaction processes of coal, Fuel, 24, 269–284, 1950.

Waquet, F., Peers, F., Ducos, F., Goloub, P., Platnick, S., Riedi, J., Tanré, D., and Thieuleux, F.: Global analysis of aerosol properties above clouds, Geophys. Res. Lett., 40, 5809–5814, https://doi.org/10.1002/2013GL057482, 2013.

Wu, H., Taylor, J. W., Szpek, K., Langridge, J. M., Williams, P. I., Flynn, M., Allan, J. D., Abel, S. J., Pitt, J., Cotterell, M. I., Fox, C., Davies, N. W., Haywood, J., and Coe, H.: Vertical variability of the properties of highly aged biomass burning aerosol transported over the southeast Atlantic during CLARIFY-2017, Atmos. Chem. Phys., 20, 12 697–12 719, https://doi.org/10.5194/acp-20-12697-2020, 2020.

https://doi.org/10.5194/acp-2022-501
Preprint. Discussion started: 29 August 2022

Yang, M., Huebert, B. J., Blomquist, B. W., Howell, S. G., Shank, L. M., McNaughton, C. S., Clarke, A. D., Hawkins, L. N., and et al., L. M. R.: Atmospheric sulfur cycling in the southeastern Pacific – longitudinal distribution, vertical profile, and diel variability observed during VOCALS-REx, Atmos. Chem. Phys., 11, 5079–5097, https://doi.org/10.5194/acp-11-5079-2011, 2011.

Yokelson, R. J., Susot, R. A., Ward, D. E., Reardon, J., and Griffith, D. W. T.: Emissions from Smoldering Combustion of Biomass Measured by Open-Path Fourier Transform Infrared Spectroscopy, J. Geophys. Res., 102, 865–877, 1997.

Yokelson, R. J., Crounse, J. D., DeCarlo, P. F., Karl, T., Urbanski, S., and et al., E. A.: Emissions from biomass burning in the Yucatan, Atmos. Chem. Phys., 9, 5785–5812, 2009.

Zhang, J. and Zuidema, P.: Sunlight-absorbing aerosol amplifies the seasonal cycle in low-cloud fraction over the southeast Atlantic, Atmos. Chem. Phys., 21, 11 179–11 199, https://doi.org/10.5194/acp-21-11179-2021, 2021.

Zhang, L., Segal-Rozenhaimer, M., Che, H., Dang, C., III, A. J. S., Lewis, E. R., Dobracki, A., Wong, J. P. S., Formenti, P., Howell, S. G., and Nenes, A.: Light Absorption by Brown Carbon over the South-East Atlantic Ocean, Atmos. Chem. Phys. Discuss., https://doi.org/10.5194/acp-2021-1000, 2022.

Zhang, Q., Jimenez, J. L., Worsnop, D. R., and Canagaranta, M.: A Case Study of Urban Particle Acidity and Its Influence on Secondary Organic Aerosol, Environ Sci. Technol., 41, 3213–3219, https://doi.org/10.1021/es061812j, 2007.

Zheng, B., Chevallier, F., Ciais, P., Yin, Y., and Wang, Y.: On the role of the flaming to smoldering transition in the seasonal cycle of African fire emissions, Geophys. Res. Lett., 45, 11,998– 12,007, https://doi.org/10.1029/2018GL079092, 2018.

Zheng, G., Sedlacek, A. J., Aiken, A. C., Feng, Y., B.Watson, T., Raveh-Rubine, S., Uin, J., R.Lewis, E., and Wang, J.: Long-range transported north American wildfire aerosols observed in marine boundary layer of eastern North Atlantic, Env. Inter., 139, https://doi.org/10.1016/j.envint.2020.105680, 2020.

Zhou, S., Collier, S., Jaffe, D. A., Briggs, N. L., Hee, J., III, A. J. S., Kleinman, L., Onasch, T. B., and Zhang, Q.: Regional influence of wildfires on aerosol chemistry in the western US and insights into atmospheric aging of biomass burning organic aerosol, Atmos. Chem. Phys., pp. 2477–2493, https://doi.org/10.5194/acp-17-2477-2017, 2017.

Zuidema, P., Redemann, J., Haywood, J., Wood, R., Piketh, S., Hipondoka, M., and Formenti, P.: Smoke and Clouds above the Southeast Atlantic: Upcoming Field Campaigns Probe Absorbing Aerosol's Impact on Climate, Bull. Am. Meteor. Soc., 97, 1131–1135, https://doi.org/10.1175/bams-d-15-00082.1, 2016.

Zuidema, P., Sedlacek III, A. J., Flynn, C., Springston, S., Delgadillo, R., Zhang, J., Aiken, A. C., Koontz, A., and Muradyan, P.: The Ascension Island Boundary Layer in the Remote Southeast Atlantic is Often Smoky, Geophys. Res. Lett., 45, 4456–4465, https://doi.org/10.1002/2017gl076926, 2018.

https://doi.org/10.5194/acp-2022-501
Preprint. Discussion started: 29 August 2022

Atmospheric Chemistry and Physics Discussions

Table 1. Comparison to other published $\frac{BC}{\Delta CO}$ ratios

Fuel/Geographic Source	$\frac{BC}{\Delta CO} * 10^{-3}$	reference
savannah	2-15	Vakkari et al. (2018)
grass	10-17	Vakkari et al. (2018)
savannah	7.9	Andreae (2019)
agriculture	5.6	Andreae (2019)
savannah	5.9	Akagi et al. (2011)
agriculture (crop residue)	7.4	Akagi et al. (2011)
NW African agriculture, smouldering	7.2	Capes et al. (2008)
southern Africa (SAFARI)	7.0	Formenti et al. (2003)
Ascension Island, August	8.7-13.4	Wu et al. (2020)
this study	9.6	

all $\frac{BC}{\Delta CO}$ values are dimensionless. Most CMIP6 models rely on the Akagi et al. (2011) emission factors.

Table 2. Comparison of level-leg mean values to CLARIFY

	CLARIFY	September 2016	31 August 2017
BC mass frac. (%)	13-15	5.4-9.2	7
BC num. frac. (%)	39 ± 7	15-40	30-35
SSA_{530}	~0.84	0.85-0.88	0.83-0.86
MAC_{660} ($m^2\ g^{-1}$)	11-12	9.5-11.5	10-11.5
OA:BC mass	4-5	$10\text{-}14 \pm 2$	8-10
LDMA median diam. (nm)	232	140-180	180-200
BC core diam. (nm)		130-150	150-160
IN frac. (%)	100	~ 25	~ 50
f44	0.19-0.22	0.18-0.22	0.215
$\frac{OA}{\Delta CO} * 10^{-2}$	4.2-6.4	6-11	6.5-11.5

CLARIFY free-tropospheric values taken from Wu et al. (2020) and Taylor et al. (2020), based on CLARIFY 033-039 and 045-051 flights.

https://doi.org/10.5194/acp-2022-501
Preprint. Discussion started: 29 August 2022

Atmospheric Chemistry and Physics Discussions

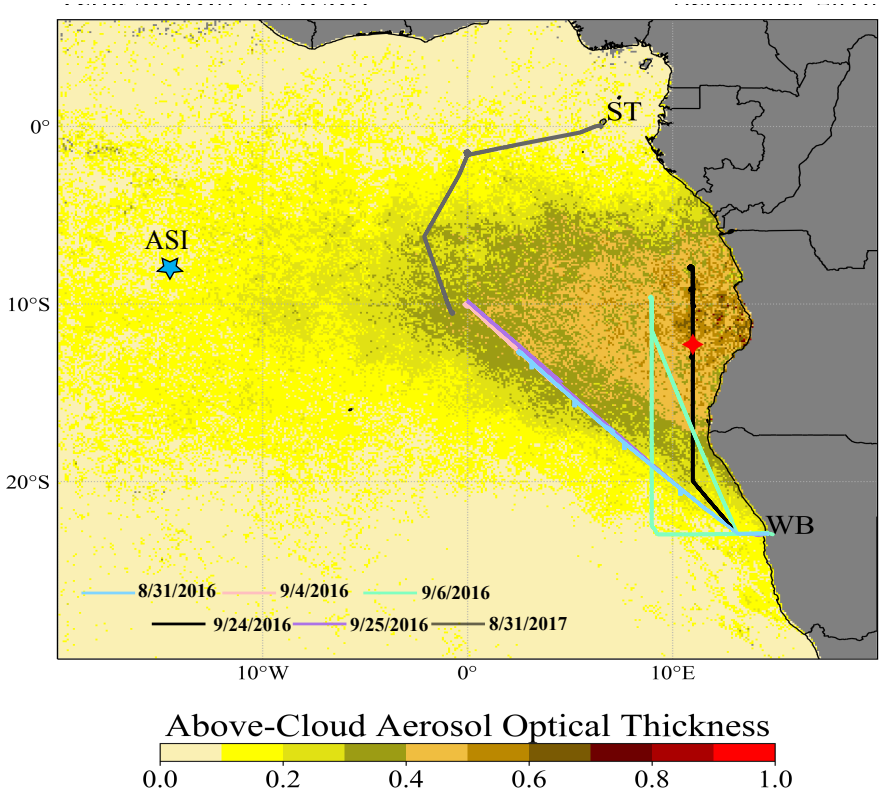

Figure 1. Terra MODIS Above Cloud Aerosol Optical Depth (Meyer, 2015) for September 2016 overlaid with the tracks of the 6 flights selected for this study. The location of the profile shown in Fig. 10 is indicated with red diamonds. ST=Sao Tome; WB=Walvis Bay; ASI=Ascension Island.

https://doi.org/10.5194/acp-2022-501
Preprint. Discussion started: 29 August 2022

Atmospheric Chemistry and Physics Discussions

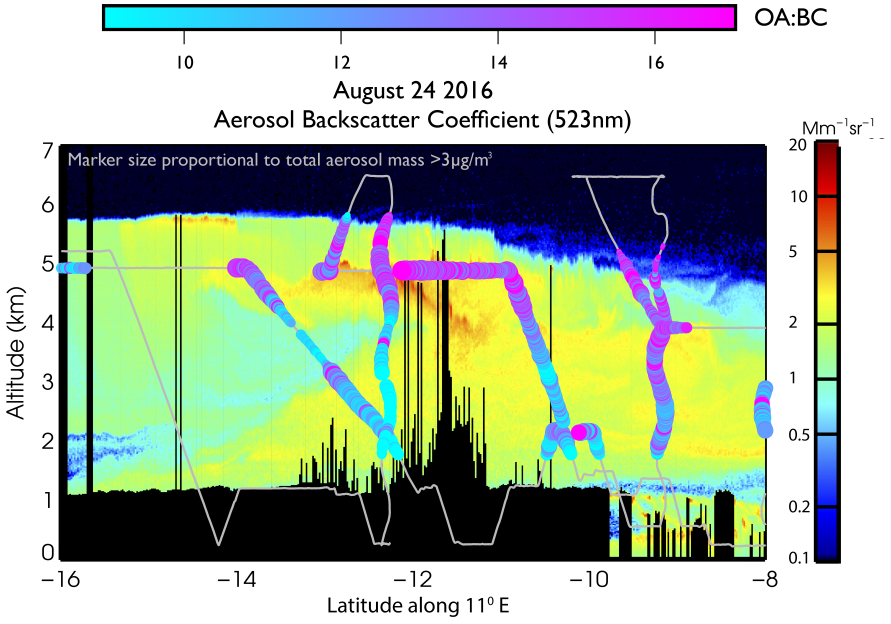

Figure 2. 24 September 2016 flight track with colorized OA:BC mass ratios superimposed on High Spectral Resolution Lidar-2 523 nm aerosol backscatter imagery collected along 11°E by the overflying ER-2 plane, near in time to the P-3 plane location's at 10°S.

https://doi.org/10.5194/acp-2022-501
Preprint. Discussion started: 29 August 2022

Atmospheric Chemistry and Physics Discussions

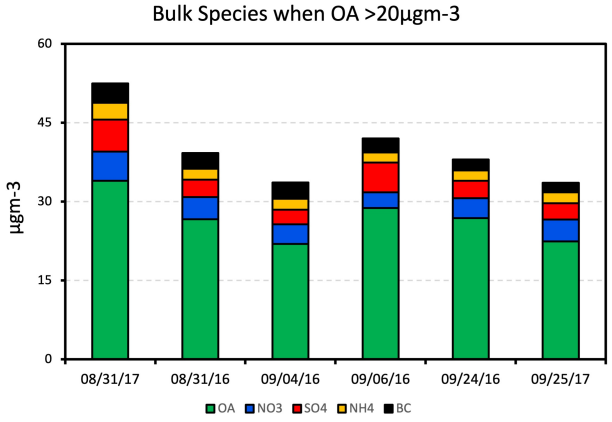

Figure 3. Mass of the bulk chemical species for each flight, for OA>20 μg m^{-3} only.

https://doi.org/10.5194/acp-2022-501
Preprint. Discussion started: 29 August 2022

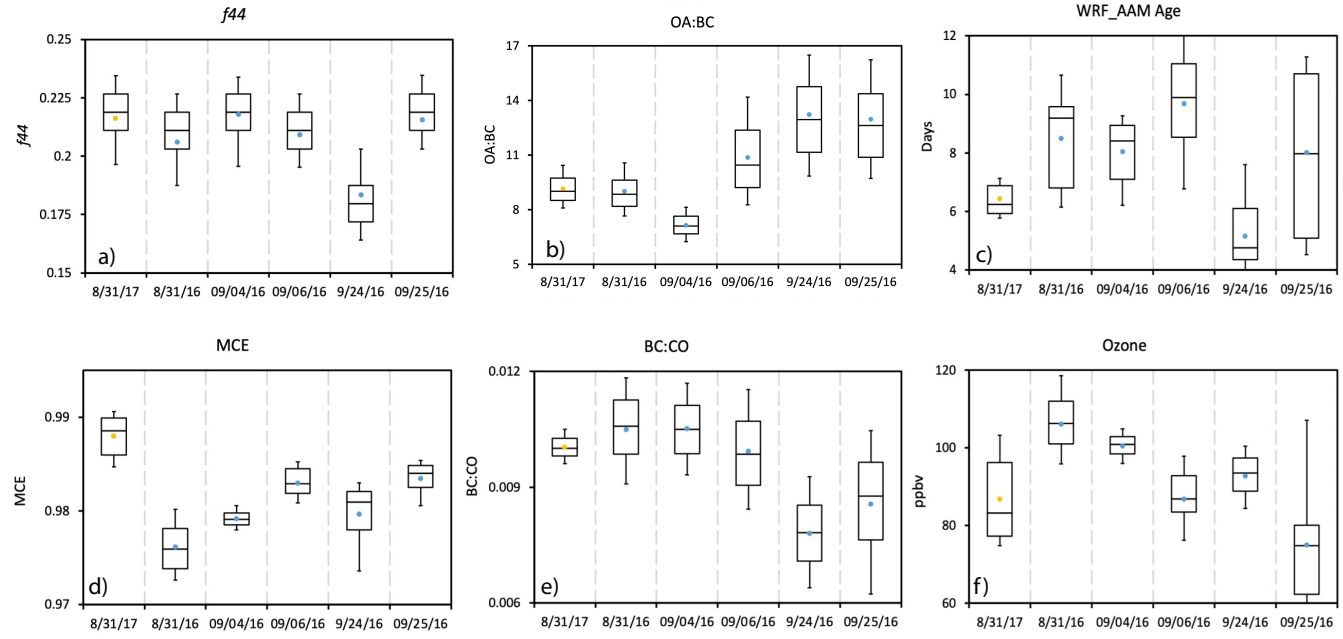

Figure 4. a) *f44*, b) OA:OC, c) model-derived time since emission (age), d) modified combustion efficiency (MCE), e) black carbon to carbon monoxide ($\frac{BC}{\Delta CO}$) non-dimensionalized ratios, and f) ozone, all for each indicated flight. Whiskers represent the 10th and 90th percentiles, boxes illustrate the 75th and 25th percentiles with a line indicating the median and yellow (2017) and blue (2016) filled circles representing the mean. OA>20 μg m^{-3} only.

https://doi.org/10.5194/acp-2022-501
Preprint. Discussion started: 29 August 2022

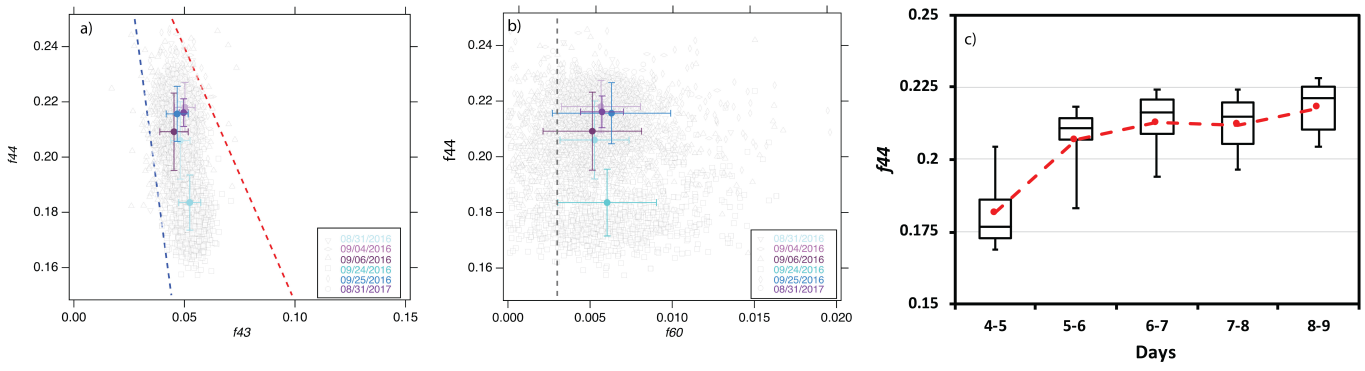

Figure 5. a) *f44* versus *f43* for the six flights where OA $>$ 20 μg m^{-3}. Averages ($\pm$ standard deviation) are colored by flight, grey boxes indicate individual data points. b) similar to a), for *f44* vs *f60*. Blue and red dashed lines define the parameters for ambient oxygenated OA, following Ng et al. (2010). c) *f44* versus the model-derived physical age for the six flights combined.

https://doi.org/10.5194/acp-2022-501
Preprint. Discussion started: 29 August 2022

Atmospheric Chemistry and Physics Discussions

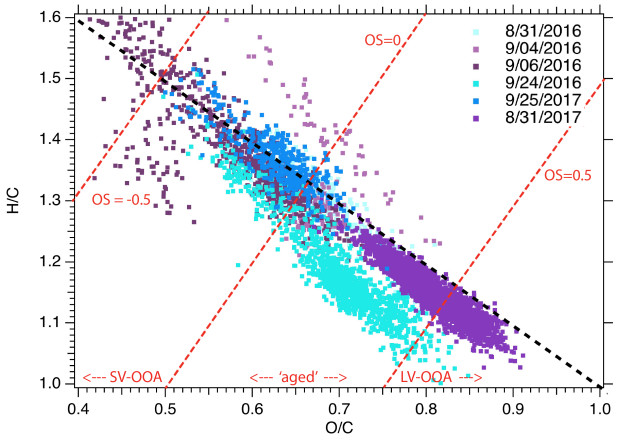

Figure 6. Hydrogen to carbon (H:C) molar ratio versus oxygen to carbon (O:C) molar ratio, colorized by flight, shown at the native 5-second time resolution. Superimposed are lines of constant oxidation state (OS (2* O:C - H:C); Kroll et al., 2011), used to define semi-volatile, aged and low-volatile regimes.

https://doi.org/10.5194/acp-2022-501
Preprint. Discussion started: 29 August 2022

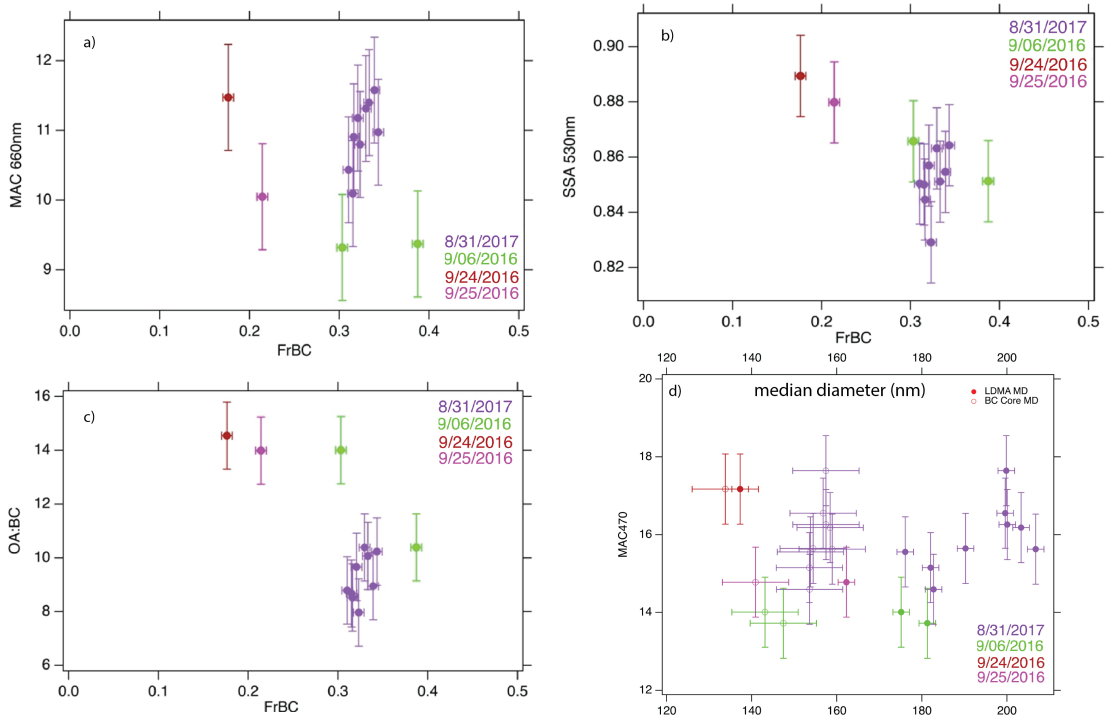

Figure 7. a) Mass absorption coefficient (MAC; units of m^2 g^{-1}) at 660 nm wavelength versus the fraction of black-carbon-containing particles (FrBC; SP2 total particle count/LDMA total particle count), for the level legs identified in Table S2, colored by flight day. b) same as a) but for SSA_{530nm} versus FrBC. c) same as a) but for OA:BC versus FrBC. d) MAC_{470nm} versus LDMA median and BC core mass median diameter. All for the level legs listed in Table S2.

https://doi.org/10.5194/acp-2022-501
Preprint. Discussion started: 29 August 2022

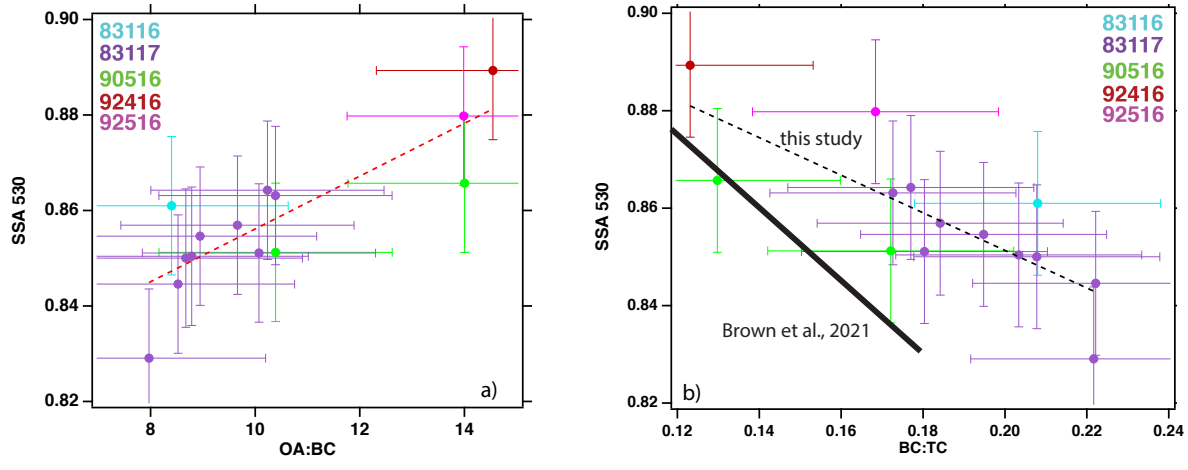

Figure 8. a) Level-leg-mean ± standard deviation values for SSA_{530nm} versus the OA:BC mass ratio, colored by flight. The best-fit line is represented by SSA=0.801+0.0055*(OA:BC) (r=0.84). b) same as a) but for SSA_{530nm} versus the BC:TC mass ratio, where TC=BC+organic carbon. The best-fit line is SSA= 0.93-0.39*(BC:TC), (r= -0.79). Times and spatial ranges of the level-legs provided in Table S1. Also shown is the SSA parameterization put forth within Brown et al. (2021), namely SSA_{550nm}=0.969-0.779*(BC:TC), where TC=BC+organic carbon (OC) and OC is estimated from OA:OC=1.26*O:C+1.18 (Aiken et al., 2008).

https://doi.org/10.5194/acp-2022-501
Preprint. Discussion started: 29 August 2022

Atmospheric Chemistry and Physics Discussions

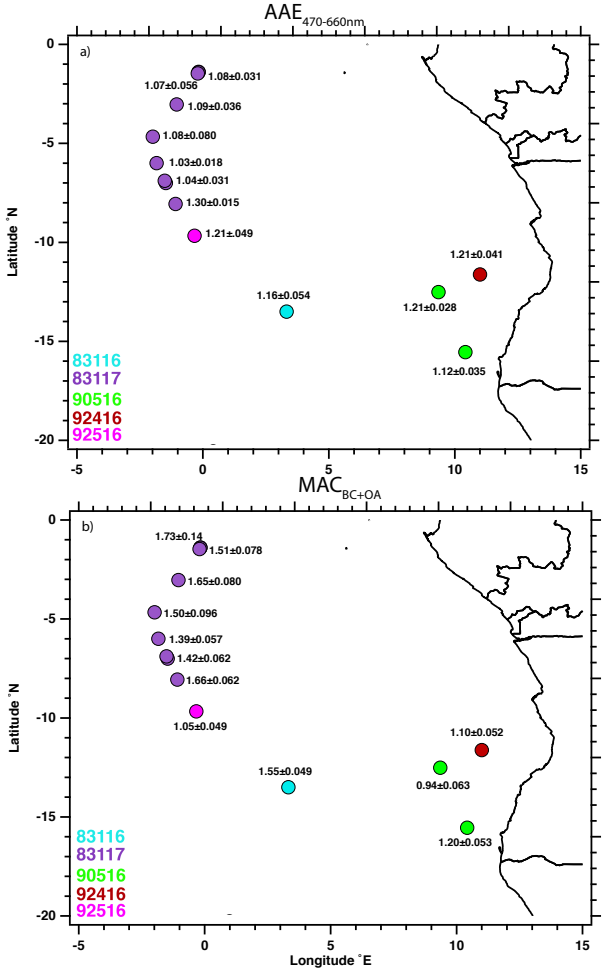

Figure 9. a) Absorption Angstrom exponent (470-660 nm), b) Mass absorption coefficient (MAC_{OA+BC}, in units of $Mm^{-1}/(\mu g\ m^{-3})$ at 470nm, for the same level legs shown in Fig. 13, similarly colorized by flight.

https://doi.org/10.5194/acp-2022-501
Preprint. Discussion started: 29 August 2022

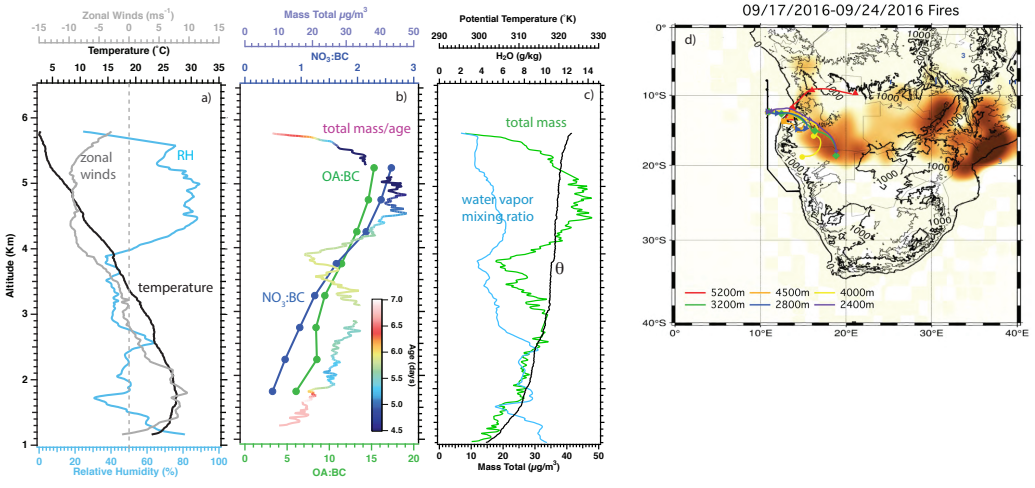

Figure 10. 24 September, 2016 (12.34°S, 11°E) vertical profiles of a) relative humidity (%; blue), zonal winds (m s^{-1}; grey) and temperature (°C), and b) organic aerosol to black carbon mass ratio (OA:BC; green), total nitrate to black carbon ratio (NO_3:BC; blue) averaged every 500 m (approximately 2 minutes of data), and c) total mass concentration (OA + BC + SO_4 + NO_3 + NH_4 in μg m^{-3}; 1Hz resolution) colored by aerosol age. d) HYSPLIT trajectories superimposed on map of fires detected between 9/17/2016-9/24/2016.

https://doi.org/10.5194/acp-2022-501
Preprint. Discussion started: 29 August 2022

Atmospheric Chemistry and Physics Discussions

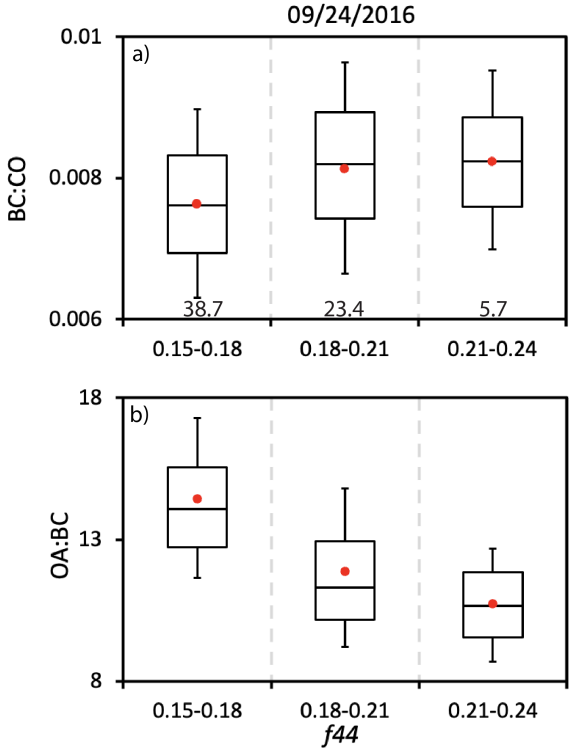

Figure 11. a) $\frac{BC}{\Delta CO}$ ratios (dimensionless) as a function of *f44* for the 9/24/2016 flight. The number of minutes contributing to each *f44* bin is stated at bottom of panel. b) same for OA:BC. Whiskers represent the 10th and 90th percentiles, boxes illustrate the 75th and 25th percentiles with a line indicating the median and a red filled circle the mean. OA>20 μg m^{-3} only.

https://doi.org/10.5194/acp-2022-501
Preprint. Discussion started: 29 August 2022

Atmospheric Chemistry and Physics Discussions

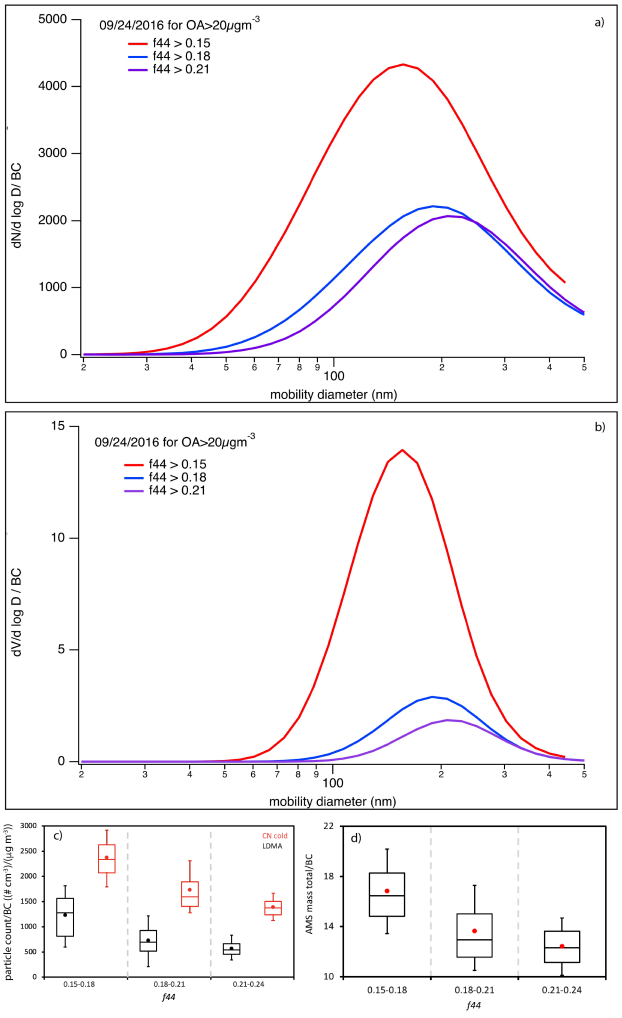

Figure 12. a) 24 September, 2016 LDMA-derived number particle size distribution as a function of three *f44* bins, normalized by BC. b) same as a) but for the LDMA-derived volume particle size distribution. c) LDMA and CN particle number concentration and d) non-BC mass total (OA + SO_4 + NO_3 + NH_4 in μg m^{-3}), with respect to BC, as a function of the three *f44* bins. All data are selected from OA >20 μg m^{-3}.

https://doi.org/10.5194/acp-2022-501
Preprint. Discussion started: 29 August 2022

Atmospheric Chemistry and Physics Discussions

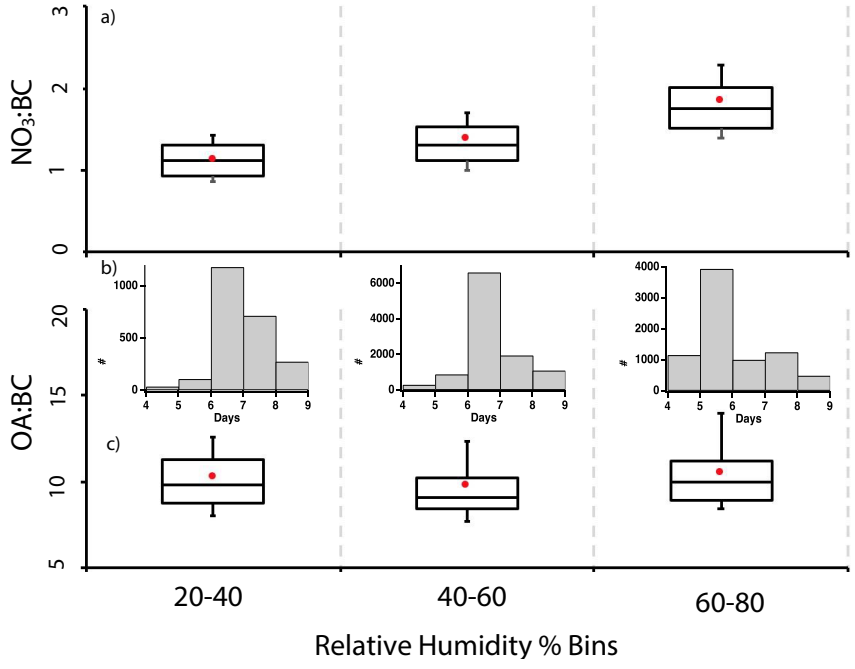

Figure 13. a) NO_3:BC and c) OA:BC mass ratios for the 6 selected flights as a function of relative humidity, for OA>20 μg m^{-3} at STP. The 10th, 25th, median, 75th and 90th percentiles are indicated using box-whiskers, the mean with solid red circle and marker. b) corresponding distribution of aerosol ages within each relative humidity range, with the y-axis indicating the number of 1-sec samples.